DUBBLE-II Project

Conceptual Design Report for the

Hard X-ray Spectroscopy BEAMLINE (BM14)

October 2016

DUBBLE-XAS-CDR-2016-002

Prepared by

Roelof van Silfhout

With input from

Guy Luijckx, Geoff Mant

Reviewers and Approvals

Document Updates

July 2017

Acknowledgements

Executive Summary

A concept for a state-of-the-art x-ray spectroscopy beamline is presented. A flexible arrangement of achromatic focusing optics has been selected that provide a range of focusing conditions enabling a wide variety of experiments with x-rays. The beamline will serve the Dutch and Flemish x-ray spectroscopy users for the next 10 years once the upgraded ESRF synchrotron radiation source resumes operations in 2020. The existing combination of measurement techniques, gas rigs and sample environments will all be available as before.

The proposed design has the emphasis on ease of operation and flexibility in terms of complementary techniques that enable comprehensive studies of samples in both dynamic as static environments. With the significant beam size reduction and modest intensity increase of the upgraded source, the new beamline is well positioned to allow users to investigate samples with high-spatial resolution and high-energy resolution. Introduction of continuous energy scanning modes together with the increase in beam flux at all energies will aid dynamic studies. Removal of many vacuum windows provides users with x-ray energies down to 2.4 keV, opening up an important window for the study of biologically important materials. Full use of the fact that the new source produces a significant flux at X-energies of above 30 keV is made by extending the high-energy limit beyond 60 keV, which will enable new methods to be introduced. An option to create a complete windowless beamline with a dedicated soft (or tender) x-ray monochromator is planned for.

Thanks to the high-quality source and refined focusing optics, the beamline provides an excellent microprobe for experiments on fluorescence analysis (photon-in/photon-out, compositions of buried components, compositional mapping/imaging, oxidation state mapping and micro tomography. Adding in the large increase in coherent flux makes the beamline suitable for medium resolution coherent diffraction imaging experiments, a further method to provide enhanced contrast in addition to anomalous scattering. The use of grazing incidence XAFS studies would provide a very high selectivity for cations and anions on surfaces (both model systems and natural crystallites).

The concept is flexible enough to allow the introduction of specialist monochromators and additional optics with the aim of enlarging the already large energy range even further. The use of a combined toroidal/flat mirror makes the link between the current horizontally unfocused operation and high flux, fully focused operation that provides up to two orders of magnitude increase in monochromatic flux.

The report recommends investment into state of the art x-ray mirrors that feature low slope errors with appropriate mirror benders with the aim of preserving the large gain in brilliance of the upgraded source. For high flux operation, a revised monochromator cooling will be required in order to achieve uncompromised delivery of the highest quality monochromatic beams.

Glossary

2PW - 2 Pole Wiggler

3PW - 3-pole Wiggler

BM26A/B - Existing DUBBLE beamlines A (spectroscopy) & B (SAXS/WAXS)

BW - Band Width

CRG - Collaborative Research Group

CXDI - Coherent X-ray Diffraction Imaging

DCM - Double Crystal Monochromator

ESRF - European Synchrotron Radiation Facility

EXAFS - Extended Absorption Fluorescence Spectroscopy

FE - Finite Element

SAXS - Small Angle X-ray Scattering

SBM - Short Bend Magnet

SR - Synchrotron Radiation

SRW - Synchrotron Radiation Workshop

TFM - Toroidal Focusing Mirror

VCM - Vertically Collimating Mirror

WAXS - Wide Angle X-ray Scattering

XAFS – X-ray Absorption Fluorescence Spectroscopy

XANES – X-ray Absorption Near Edge Spectroscopy

XRT – X-ray Ray Tracing

Coordinate System

A right-handed coordinate system is used throughout this document in which the positive *y*-direction is pointing in downstream and along the centre of the fan of radiation. The positive *z*-direction is pointing up out of the horizontal plane of the electron orbit.

Table of contents

Intentionally left blank

1. Introduction

The Dutch Research Council (NWO) has invested in access to synchrotron radiation (SR) for over 35 years. First access to SR for Dutch users was achieved by funding of a SAXS beamline at the Synchrotron Radiation Source (SRS) (Daresbury, UK) which also gave Dutch users access to other SRS beamlines. As a result there is a strong Dutch user community in X-ray spectroscopy, interface diffraction and time-resolved SAXS. The closure of the SRS required access to another SR source for which the ESRF was chosen and through collaboration with Flemish partners the DUBBLE project, was established. The DUBBLE BM26A beamline has been in operation for nearly 11 years. In this time it has produced data for close to 400 manuscripts and that number is growing at a rate of about 40 manuscripts/year with an average journal impact factor of around 6. The main technique is time-resolved x-ray absorption and fluorescence spectroscopy (XAFS). Over the years the infrastructure has evolved in such a way that complicated sample environments and auxiliary non-X-ray based techniques can be applied. In addition users can perform x-ray diffraction (XRD) and small angle x-ray scattering (SAXS) (quasi-) simultaneous and an elaborate gas mixing/pressure system is available for catalysis experiments. An option for confocal microfocus XRF/XANES using capillary lenses has been developed. This has produced both 3-D data as well as allowed depth resolved studies of chemical composition. A KB system is being commissioned and will be made available in 2017 for conventional microfocus EXAFS experiments.

After the ESRF machine upgrade, planned for 2019/20, it is no longer possible to accommodate two beamlines on a single port and BM26A beamline must be relocated to a new bending magnet port. There are two main reasons why moving BM26A - as opposed to moving BM26B (SAXS/WAXS) - to a new port is preferred. First, the SAXS/WAXS beamline has a dedicated experiments hutch that is bespoke and large enough to accommodate a range of camera lengths. Second, the optical components for the SAXS beamline are positioned closer to the position of the smaller x-ray fan produced by the new source. Finally, the BM26A beamline currently receives its radiation from a 0.4 T bending magnet compared to the SAXS line (BM26B) that has a 0.8 T bending magnet. With the suggested relocation to a new 0.8T bending magnet source the new spectroscopy beamline will benefit from a higher photon flux.

This document captures the key beamline parameters for a proposed state-of-the-art x-ray spectroscopy beamline located at one of the bending magnet ports of the upgraded ESRF synchrotron radiation source to replace BM26A. We then continue with a close look into the source options provided by the ESRF for CRGs with the aim to select the best one for spectroscopy use. After the choice of source we proceed by considering each beamline component in sequence. A detailed beamline layout is presented in which key design decisions are described and contrasted with alternative approaches. Where appropriate, we have included potential future upgrades that could provide new capabilities without compromising the spectroscopy capability of the beamline.

The presented concept focuses on experiments that require fine control over photon beam energy whilst providing a very flexible approach to the focusing conditions of the beam making full use of the upgraded source without restricting the detailed experimental techniques.

To support the design choices we have made extensive use of ray trace calculations (XRT & SRW) [1]. In most of our calculations we have combined both insertion device ***and*** surrounding dipole sources in order to represent the expected behaviour as close as possible.

2. Scientific requirements

X-ray absorption and fluorescence spectroscopy is one of the most versatile techniques based on synchrotron radiation. It makes full use of the broad energy spectrum provided by the source to provide a direct insight into the

electronic structure and local environments at an atomic level around target atoms. These unique properties make such a beamline suitable for a wide range of applications in catalysis, nucleation, materials science, environmental and earth science and biological systems. Due to the smooth variation of flux versus photon energy bending magnet beamlines are particular suitable to act as sources for a spectroscopic beamline. The significant increase in source brilliance will also great opportunities to image the distribution of elements, compounds with high spatial resolution (chemical mapping). Advances in beamline design combined with the high energy of the synchrotron enable the provision of a wide range of energies and the envisaged facility will provide photon energies from 500 eV to 65 keV covering K-edges from Oxygen to Gold. This large range is particularly notable as it combines the so called 'tender'and hard x-ray ranges allowing users to study elements from Oxygen to Gold. The extension to the lower end of the energy range is exciting not only will be K-edges of important elements be accessible but users will also be able to make use of the so called water window.

Every synchrotron will feature one or more dedicated spectroscopy beamlines, therefore users will primarily focus on the quality of the x-ray beam, energy range provided and available infrastructure in terms of sample environment, complementary experimental methods and instrumentation.

BM26A is a good example of a facility in which user driven instrumentation and complementary techniques has led to an excellent environment, which is oversubscribed and producing an above average output of high impact papers. The new spectroscopy beamline will target a wider range of energies, provide a higher flux density and the ability to increase the time resolution over thirtyfold by introducing a dedicated quick scan mode. At the same time the proposed optical setup will be fairly flexible as to allow further optical components to be inserted at a later stage.

The beamline is to provide a versatile and highly productive facility for X-ray Absorption/Fluorescence Spectroscopy for a wide range of scientific disciplines:

- Catalysis and energy science
- Earth & Environmental science
- Nanomaterials and condensed matter research
- Life science and biology

To achieve the above goals and to attract (and continue to do so) the best science the proposed beamline must feature:

- Access to a wide range of elements supporting more scientific disciplines
- Improved temporal and spatial resolution (time resolved spectroscopy & chemical mapping)
- Quick beamline alignment and energy range/operational mode change
- Availability of complementary methods for sample analysis (*e.g.* small/wide angle scattering, mass spectrometry, Raman spectroscopy, electron yield measurement)
- Various geometries: transmission, fluorescence and grazing incidence
- Addition of x-ray emission spectroscopy
- Variety of sample environments (oven, cryostat, high pressure, …)
- In situ measurements: electrochemical cells, gas and solution flow-through cells

Key design decisions are indicated by red arrows (➔), sections with require further action are marked with ☒. Optional items that enhance and extend the use of the beamline are highlighted by ⓘ. The ❖ -symbol is used to indicate some useful numerical results.

Key information regarding the ESRF machine upgrade and the new insertion device specifications were taken from an ESRF briefing document written by J. Chavanne [2].

3. Key design choices

The performance of the beamline is dependent on a small set of key design parameters that are discussed in the sections below. Once defined, these choices shape the detailed optics design.

3.1 Radiation source

➔ *It is proposed to use the two-pole Wiggler (2PW) as the insertion device for the new spectroscopy beamline.*

The ESRF EBS upgrade has a considerable effect on the operation of CRG beamlines. The new low-emittance lattice proposed is using multiple bending magnets with a reduced magnetic field as opposed to the magnets in the old lattice. To overcome this lack of a suitable source with similar critical energy for future CRGs, the ESRF has proposed three schemes (table 1) that use dedicated insertion devices located at a position close to the existing bending magnet. In addition, the neighbouring dipoles are available with magnetic fields of 0.4 and 0.6 T.

Insertion Device	Number of magnet poles	Horizontal Divergence (mrad)	Magnetic Field (T)
Short Bending Magnet (SBM)	1	2	0.856
Two pole Wiggler (2PW)	2	1.7	0.856/0.856
Three pole Wiggler (3PW)	3	1.6	0.5/0.856/0.5

Table 1: Overview of insertion devices available to CRGs after the ESRF upgrade.

Of the three schemes only one (SBM) uses a canted magnet arrangement to avoid interference of radiation from neighbouring bending magnets. The highest flux across the energy range is provided by the 2PW which will be double that of the SBM whereas the 3PW output will lie between these two due to the fact that two of its poles are only 0.5 T in strength. Figure 1 shows the maximum flux expected for each source together with that of BM26A, which has a 0.4 T bending magnet as its source. For the case of the 2PW only the contribution of the insertion device is shown.

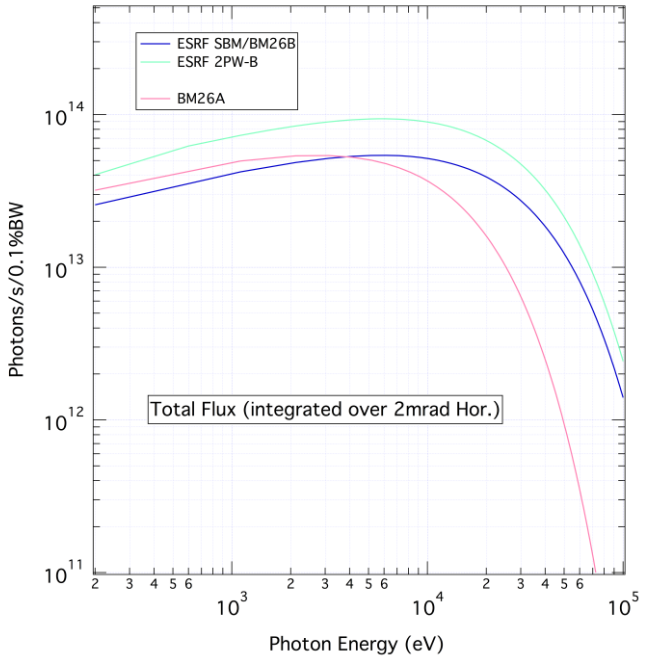

Figure 1: Flux comparisons for the two EBS options and the existing source at BM26A for photon energies between 200 eV and 100 keV.

For energies lower than about 4 keV, the SBM option will have a lower flux than currently available at BM26A. The curve for the 2PW device does not take into account the contribution of the bending magnet that partially overlaps with the available fan of radiation. The total flux curves have been calculated with the usual assumption of a 0.1% Band Width (BW) which is approx. one order of magnitude larger than that of a Si(111) monochromator. Therefore, the expected flux at the sample will be below 10^{13} photons/s. In practical cases - where a smaller acceptance angle is used in combination with two (non-ideal) mirrors - the expected flux is in the range 10^{11} - 10^{12} photons/s.

Compared to the existing source, the upgraded machine offers a significant reduction in electron beam cross-section and horizontal emittance. In table 2, we compare the changes between the current source and that of the upgraded one. Looking at the so called beta functions which describe the horizontal and vertical size of the electron beam, it seems that in the new lattice the electron beam cross section at the location for CRG ports is small compared to other positions around the lattice. Therefore one can expect significant gains in brilliance of the upgraded facility, which will particularly benefit experiments that require small and bright beam spots for sample probing provided that suitable focusing optics is used.

The coherent fraction of the beam will be significantly larger; we will investigate this aspect later in this report.

	Current High/Low Beta	After Upgrade
Hor. Emittance (ε_x) [pmrad]	4000	130
Vert. Emittance (ε_z) [pmrad]	5	5
Hor. RMS beam size (σ_x) [µm]	98/132	23
Vert. RMS beam size (σ_z)[µm]	11/13	3.6

Table 2: Electron beam parameters before and after upgrade

The slightly smaller horizontal divergence, the modest increase of flux combined with the large gain in brilliance provide a significant improvement compared to the current situation allowing faster data collection or measurements on more dilute samples. One could also consider increasing beamline energy resolution significantly compared to the existing BM26A beamline whilst keeping photon flux at comparable levels by opting to use Si(311) monochromator crystals throughout most of the photon energy range. There are two configurations for the 2PW (option A & B) depending on the transversal arrangement of the magnetic poles. The B-configuration aligns the 2PW radiation fan to within 0.15 mrad of the downstream bending magnet which has a stronger magnetic field compared to that of the upstream bending magnet resulting in a slightly higher flux level. Option A results in an overlap with the upstream dipole which is located close to the insertion device. The choice between the A or B option is rather subtle. One significant difference is that for the B-option the beamline will be located closer to the tunnel wall but not as close as that of the BM26B beamline (-8.7 *vs*. -10.5 mrad).

The vertical source size is not changing between the various insertion devices so there is no difference in degradation of the energy resolution. For the 2PW and 3PW insertion devices there is an overlap with one (or both) of the neighbouring dipoles. Because the vertical beam size at the dipoles is similar to that measured at the insertion device position we don't expect any degradation of the energy resolution. Due to the difference in position of the sources one can expect some detrimental performance when trying to obtain a perfectly collimated beam but this would be at the level of 1-2 nrad, which is significantly smaller than the acceptance angle of the monochromator crystals.

The 2-pole nature of the wiggler insertion device is unlike a traditional, well-studied multi-pole wiggler. The transversal separation of the two source points is a function of the viewing angle. The two source points are close together and can be brought in-line by a 0.8 mrad change of viewing angle. Along the magnetic axis the two poles have a transversal separation of approx. 27 µm. This separation is similar in size as the horizontal electron beam source size at the insertion device position. With a 0.4 mrad angular offset, the RMS horizontal source size of the 2PW will be similar to that of the SBM, which represents the smallest possible source size.

Ultimately this separation and its dependency on viewing angle will have a direct influence on the effective source size of the two-pole wiggler. Full separation to coinciding wiggler poles is achieved by changing the viewing angle 0.8 mrad from the centre point.

☒ *The close proximity of the two wiggler sources and bending magnet will raise some intriguing questions regarding the interference of the emanating beams particularly at lower energies.*

For lower energies the 2PW shows clear side peaks which are similar in nature to those seen in regular undulator source with a reduced number of poles. Its behaviour at very low energies requires a further detailed analysis.

3.2 Coherence

The reduction in the (horizontal) source size increases the transversal coherence length of the source. For a given source size σ one can expect a fully transversal coherent beam within an angle of:

$$\theta \leq \frac{\lambda}{\sigma}$$

Using the above as a measure (assuming Gaussian beam shape) one readily finds that with a typical vertical acceptance of 80 µrad (2 mm slit at 25 m) that the beam is fully coherent at beam energies below 5 keV.

The coherent fraction is found using (assuming a Gaussian beam shape):

$$\frac{I_{coh}}{I} = \frac{\lambda^2}{(4\pi)^2 \varepsilon_x \varepsilon_z}$$

where λ is the wavelength of the radiation, and ε_x, ε_y the source emittance in the horizontal and vertical. For the 2PW wiggler, we get 0.6 for λ = 2.5 Å wavelength and 0.09 for λ = 1 Å.

In order to arrive at a practical estimate of fully coherent flux we use the generic point source expression for the coherence lengths using slits:

$$\ell_{c_{x,z}} = \frac{\lambda D}{2\sigma_{x,z}}$$

At a distance (D) of 50 m from the source the coherence 'area' has a size of 110 x 625 µm^2 (*hxv*). Within this cross section the beam is fully coherent for a monochromatic beam with an energy of 12.4 keV. At 5 keV the coherence 'area' increases to 0.28 x 1.6 mm^2 (*hxv*). Often a *less* restrictive condition of partial coherence is sufficient allowing a larger beam to be used. In photon correlation spectroscopy, for example, slit width values of twice the above coherence length are used for obtaining the best signal-to-noise values. Using a secondary set of slits a range of coherence lengths can be obtained (see section 4.5) [3].

❖ *Using ray tracing we find that the fully coherent flux at 50 m distance from the source is 2x10^7 photons/s at 12 keV and 2x10^8 photons/s at 5 keV.*

The expected coherent fluxes are sufficiently high to consider static Bio-CXDI (Coherent X-ray diffraction imaging on biologically interesting samples) experiments especially considering that one can use focusing optics after the coherent fraction selecting slits allowing the coherent flux to be incident into a sub-micrometre scale volume. For comparison: a single XFEL pulse - which is almost fully coherent - has 10^9 photons.

Energy range

➔ 2.4 - 62 keV [crystal monochromator range – Si(111) & Si(311)]

➔ 400 – 3000 eV (blazed grating monochromator range – 1200 lines/mm)

Ideally, the energy range of the beamline would be as large as possible allowing users a maximum flexibility in selecting absorption edges taking into account that users are interested in a wide range of materials that span the periodic table. Realistically, this photon energy range is limited by source properties, method of monochromatisation, reflectivity of optical elements, vacuum windows, *etc.* It is our aim to match the available photon energy range available from the source as much as possible with that of the range of K-edges of *key* elements in the periodic table whilst finding solutions for technical limitations of energy selection, filtering and focusing of the radiation that result in an easy to use facility for users. For example, below 2 keV the use of a Silicon crystal monochromator becomes problematic, the options are the use of Beryl crystals or gratings. Blazed gratings are the workhorse of soft and tender X-ray facilities around the world and modern implementations promise significantly higher efficiencies that can be achieved with crystal monochromators. Due to the relatively large angle of incidence for gratings and focusing mirrors their joint implementation with a DCM monochromator and focusing optics is feasible and relatively low extra costs.

Realistically the lowest x-ray energy that can be reached with a Si(111) monochromator is close to that of the Sulphur K-edge (2.4keV). To access the Phosphor K-edge at 2.1keV, a monochromator (Bragg) angle of more than 70° is needed which requires severe design constraints in reaching high photon energies.

The upper energy limit is typically set by the magnetic field strength of the insertion device and the energy of the circulating electrons in the machine. In the case of the new insertion devices there is sufficient flux of photons with energies up to 80 keV. The ESRF could raise the magnetic field to above 1 T without major shielding issues. It that cause the critical energy would be significantly increased allowing experiments with energies well above 80 keV.

From a spectroscopy application point of view, we point out that for high-Z elements the K-shell lies too deep to be accessible and researchers use the shallower L_3 edges. However, the energy range of an L_3 EXAFS spectrum is limited by the presence of the L_2 edge. For elements with $Z < 70$ this length is typically less than 1keV (typical range of an EXAFS scan) thus K-edge measurements are preferred. For $Z > 70$ the K-edges are generally not required allowing us to select a high-energy limit of about 62 keV (K edge of Yb is at 61.3 keV).

The higher range of energies provided by the new insertion device also provides a good source for various non-destructive probing and imaging. For example, the access to photon energies above 40 keV is suitable for performing pair distribution function (PDF) measurements, which is identified as a complementary method to traditional spectroscopy studies. For high (real space) resolution measurements using the PDF method one records both the diffuse and the Bragg scattered components. Dedicated PDF studies are performed at significantly higher energies. The 2PW insertion device provides reasonable levels of flux up to 80 keV, thus extending the energy range should be kept as an option.

At these high energies, the Bragg angle of a Si(311) crystal is well below 3°, limiting the vertical divergence that can be accepted from the source. For photon energies above 50 keV the Si(333) reflection would give access to energies to about 80 keV. Filtering of the Si(111) contribution is achieved by using filters.

ⓘ *To cover for access to this energy range one could consider future addition of a focussed Laue monochromator that will be able to fill the gap between 62 and 80 keV.*

To cover the full range of energies various combinations of monochromator crystal type, mirror coating and mirror angle are required. In order to remove third harmonic contamination operation of the beamline we can identify three energy ranges that can be accessed with the same combination of optical components: 2.4-7 keV, 7-20 keV

and > 20 keV. The proposed design is optimised so that switching between the various configurations is quick and automated.

Below 2 keV (tender x-ray range) the range 500 – 2000 eV is *of great interest* to our users that often study oxides, and compounds containing F, Na, Mg and Al for example. This range of energies is readily accessible if a windowless beamline is used using focusing mirrors with a Si or Pt coating in combination with a blazed (variable line spacing) grating as opposed to a crystal monochromator. A combination of a flat mirror in combination (such as used in the SX700 design) allows scanning whilst keeping the monochromatic beam co-located with the sample. Recently multilayer coatings on top of gratings have improved the low efficiency of gratings to some extent. The use of crystals with large unit cell sizes has been ruled out due to their short lifetime in the intense x-ray beam.

In order to make it possible to change energy quickly the optical design will be optimised such that users will be able to go from tender x-rays to hard x-rays within a period of several minutes.

3.3 Beamline stability criteria

Considering the beamline as a microscope with a primary figure of merit determined by spatial resolution one can readily derive some key stability criteria assuming the simplest of optics consisting of a single focusing element. Using the full available space offered to CRG teams with the experiments hutch at about 50 m and the sample 0.05 m from the focusing optics one has a demagnification factor of 10^{-3}. With a source size of approx. 25x4 μm^2 (*hxv*) one can thus expect a focal spot size of 25x4 nm^2 assuming ideal focusing conditions. More realistic focal spot size would be 50x20 nm^2.

Considering the x-ray spot size of 50 nm and an acceptable beam drift of 10% of its size would result in a 5 nm translation. This should be respected over the duration of the scan or experiment of, say, 60 minutes. The angular tolerance is given by the 10% beam spot shift over the focal length of 0.05 m, which results in an angular stability of 100 nrad over a typical time of 1 hour.

The above figures require careful design and above all avoiding significant relative temperature changes between components. Sample and focusing optics mounting should use a common rigid structure. The best commercial DCM system available features a 54 nrad angular stability specification which is well within the above listed limit.

4. General beamline layout

An overview of the proposed beamline with its main components is shown in figure 2. For clarity filters, beam shutters, beam diagnostics and potential upgrades are not shown. The proposed design features ease of operation across the full energy range whilst making full advantage of the expected large increase of brilliance without compromising the high-energy resolution necessary for spectroscopy.

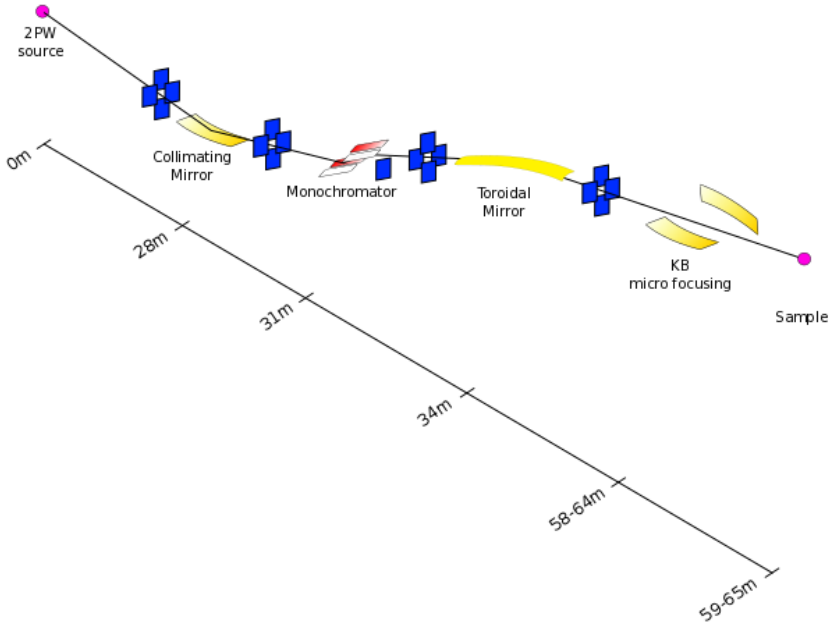

Figure 2: Proposed spectroscopy beamline layout, only key optical components are shown (not to scale).

The configuration shown has an up-up-down-down deflection geometry that provides an effective way of blocking Bremsstrahlung using a beam stop down stream of the first monochromator crystal. A detailed description of each beamline component is given in the following sections. The sample position is variable to allow for flexibility in sample environments and additional equipment. When using the toroidal mirror the focus will be located at about 60 m which is between a 1:1 and 2:1 demagnification of the source. With a slight extension of the current optics hutch the two options will be available and one could consider using two toroidal mirrors to have access to both demagnification ratios and/or two positions in the experiments hutch to cater for two setups.

The general layout requires two lead-lined hutches: one optical hutch (25.5 – 38 m) and one experiments hutch adjacent to the optical hutch (58 – 66 m) with space for control cabins and sample preparation at the back of the experiments hutch (59 – 65 m).

4.1 Front end

Currently, the ESRF CRG front end uses a 0.5 mm thick Be window placed close to the tunnel wall (25 m from the source) which seals the machine vacuum from that of the CRG beamline. A 4x1 mrad^2 aperture is used close to the source to protect vacuum chambers. Simulations were carried out to calculate the total flux and power from the *combined* sources (DQ2C, DQ1D & 2PW-B) and transmit this through the front-end window. The relatively thick window introduces a cut-off at about 5 keV; figure 3 shows ray trace results for the footprint of the beam (top) and energy spectrum (bottom) that is absorbed by the Be window.

☒ *The thickness of the frontend window should be no more than 0.2 mm thick so that 20% or more transmission is achieved for 2.4 keV photons.*

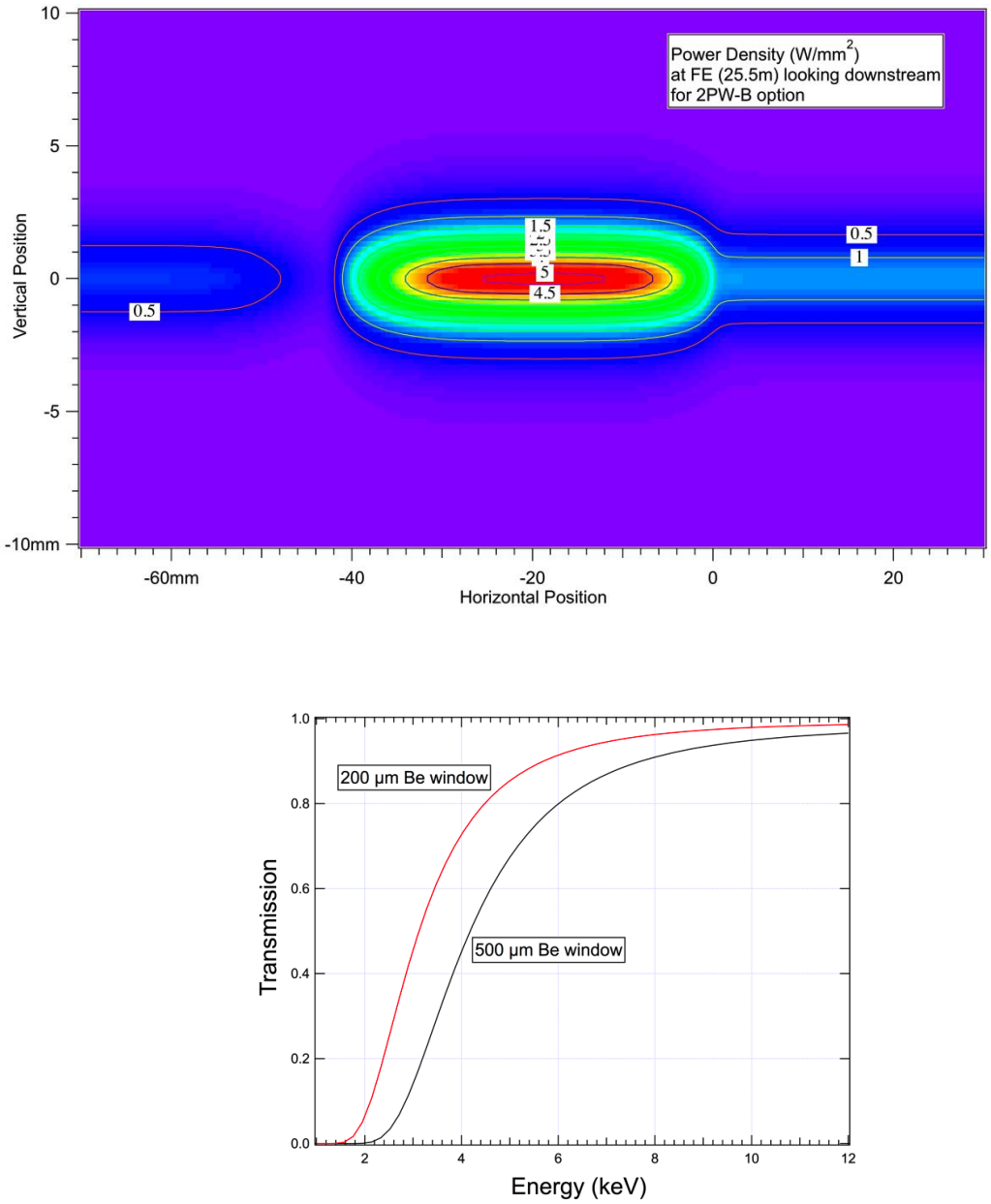

Figure 3: The top figure gives the SRW calculations for the expected power density for the combined output of the 2PW-B source together with the two adjacent dipoles that is transmitted by the front-end aperture and incident on the front-end window (DQ1D on the right, DQ1C contribution on the left). The bottom figure shows the Beryllium window absorption for low photon energy for two window thicknesses, currently the thickness (*t*) is 0.5mm.

The use of conductance limiting sections will allow the thickness of the Be windows to be minimized whilst still creating a sufficient isolation of machine and beamline vacuum. The existing 0.5 mm thick window will absorb 91 W of power and removes all x-rays below 2 keV into the experiments hutch. Efforts should focus on removal or our drastics reduction of the thickness of this window which is placed in the ESRF frontend of the beamline.

For operation with energies below 1 keV it is *required to operate the beamline window-less* through suitable differential pumping and fast acting valves for protection of the machine vacuum. Suitable methods of dealing with potential vacuum issues have already been found at the ESRF and the long acoustic delay line that is the front end allows fast acting valves to protect the machine.

4.2 Collimating Mirror

The first optical element that is exposed to the white beam is a vertically collimating mirror (VCM), which is capable of collecting the white beam cone as transmitted through the front-end mask. (The ESRF has opted to insert a 4x1 mrad^2 (*hxv*) aperture that is larger than the insertion device divergence but nevertheless useful to remove surrounding dipole contributions). The VCM has two functions:

- collimating the incident beam to provide a better energy resolution, and
- removing high-energy photons (harmonics) which would spoil spectroscopy measurements. At the same time this low-pass filter reduces the heat load on the monochromator

For a Si(111) monochromator crystals, the strongest harmonics are the third order ones. Therefore starting at 2.4 keV photon energy, the first cut-off energy is set at 7 keV, with the next one at ~20 keV. Thus one can identify three energy ranges: 2.4 - 7 keV, 7 - 20 keV and > 20 keV.

Traditionally, a 1.2 m long, flat mirror is used which is polished to the highest standards and bent into a cylindrical shape by mechanical means creating only a vertical collimation of the beam. In order to create the required energy cut-offs for the above ranges one would need two different coatings and two different angles of incidence as shown in figure 4.

Besides Si and Rh coatings a Pt coating would be required for the higher range of energies and often Pt is used instead of Rh. Compromise with this choice is that Pt absorption edges appear in the reflected beam around 11 keV causing an effective reduction in the reflectivity of the mirror. Note that the calculation represents the reflectivity for one mirror only. With a second (focusing) mirror the reflectivity for a Pt coating would approx. 0.65^2 = 0.42.

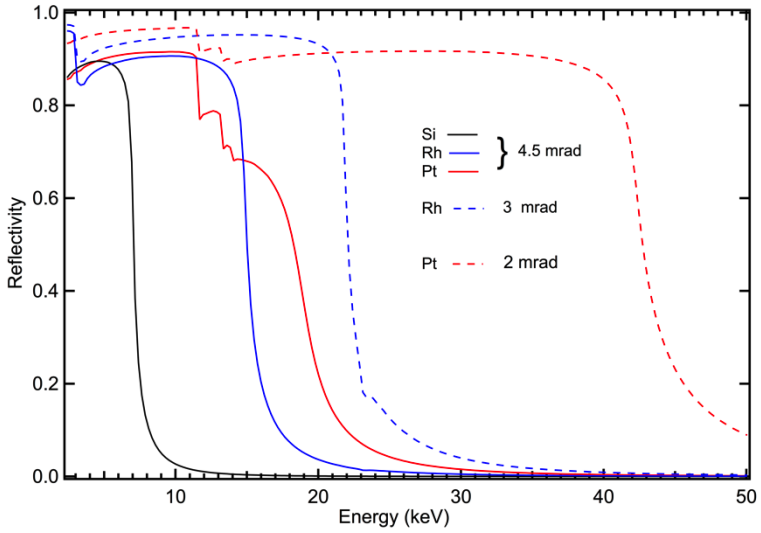

Figure 4: Mirror coating and angle of incidence for creating energy cut-offs at 7 and 20 keV.

Capturing the full 1.7 mrad horizontal divergence with the VCM located at 28 m from the source requires strips with a width of approx. 50 mm leaving no room to add a third strip. A solution proposed in the literature would make use of an Rh/Pt bilayer. In practice, the beamline would be setup to collect a fraction of the horizontal divergence especially at low energies where interference effects due to the coherent nature of the source are evident. In this case one could consider using three stripes (Si, Rh and Pt) of 30 mm width each capable of *collecting a 1.1 mrad* wide horizontal fan of radiation. Alternative coatings are: Au, Pd, Cr and Ir instead of Rh and Pt.

In order to cover the full energy range one can readily distinguish three sub-ranges for which a different mirror coating or angle of incidence must be chosen (see table 3). Although it is possible to choose different angles of incidence for the two mirrors, one would try and avoid this so that the beam near the sample is travelling in a horizontal plane.

Photon Energy	VCM coating	Angle of incidence
2.4 – 7 keV	Si	4.5 mrad
7 – 20 keV	Rh	3 mrad
20 – 40 keV	Pt	2 mrad
40 – 65 keV	-/Pt	-/1.2 mrad

Table 3: Mirror coating and angle of incidence for creating energy cut-offs.

The use of a doubly curved mirror surface would be too restrictive and compromise the capability to tune this mirror to different cut-off energies. The use of mirrors to focus the beam above energies of about 35 keV becomes problematic due to the very shallow angles.

The meridional radius of curvature is given by:

$$R_m = 2p \sin^{-1} \alpha,$$

where *p* is the source to mirror distance and *α* the angle of incidence of the beam. For practical situations this results in a radius of curvature that is rather large (>10 km) and a good gravity compensated bender will be required. Also the bending mechanism should avoid straining the reflecting surface by applying bending moments only to the bulk of the mirror body thus avoiding additional slope errors.

☒ *The power density levels on the VCM are relatively low due to the small angle of incidence. With a total absorbed power of less than 500 W an arrangement such as currently used at BM26A consisting of side cooling using liquid metal filled grooves should be sufficient. The resultant thermal 'bump' will require adjustments to the mirror bender. Such adjustments are important because they directly influence the energy resolution of the beamline.*

The Si strip should be in the centre due to the fact that it creates the largest heat loading of the mirror and a central position with equal cooling from either side will give best results.

4.3 Monochromator

➔ *Double crystal monochromators (DCMs) are well-established devices that meet the requirement to change photon energy quickly with a high resolution over a large energy range.*

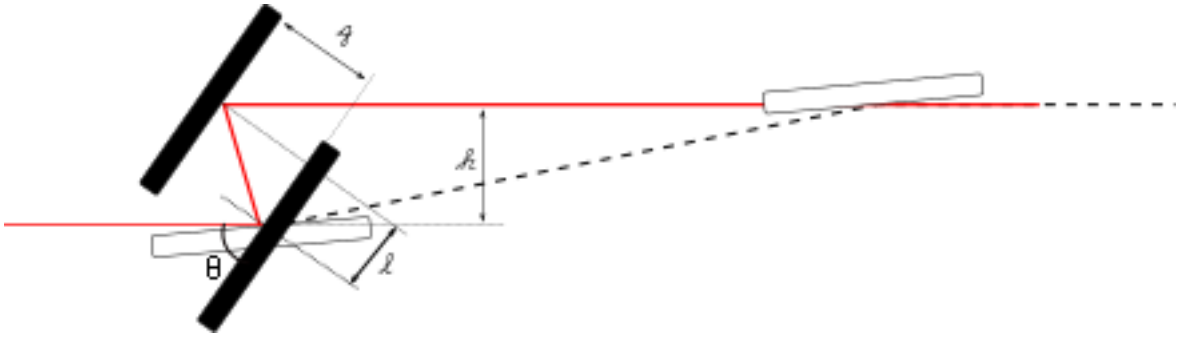

Figure 5: DCM setup geometry for low (filled) and high (open) energy setting.

The fixed offset of DCM will be maintained by adjusting the gap between the two crystals during energy scans appropriately (see below). Rather than moving the second crystal to capture the beam reflected by the first crystal a long second crystal will be used allowing the beam 'to walk' along its surface. In figure 5, we have superimposed the location of the monochromator crystals for the lowest (black filled rectangles) and highest energy (white filled rectangles) setting for the proposed energy range of 2.4 - 62 keV. From this diagram it is clear that (apart from the Bragg angle rotation) the crystal gap and crystal translation settings are energy dependent if one wants to keep the exiting beam at the same height. The two relationships for a DCM with a fixed exit height (h) are:

$$\ell = \frac{h}{2\sin\theta}$$

$$g = \frac{h}{2\cos\theta}$$

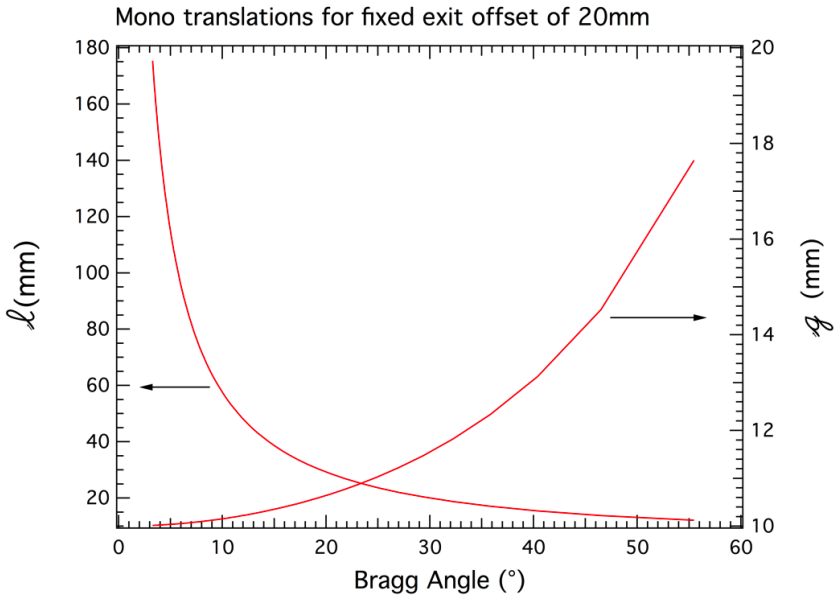

Figure 6: Monochromator translations for second crystal required for fixed exit operation

Lower energies would cause blockage of the incident beam by the second crystal whereas for higher energies the incidence angle becomes to small to capture a significant amount of beam. For a fixed exit operation mode the gap (g) between the two crystals must be adjusted. With a beam offset (h) of 20mm and crystal length (L) of 50 mm the full range of Bragg angles (θ) from 56° to 5° is available. To cover the required energy range one would need two different sets of crystals and it is proposed to use a side by side combination of Si(111) and Si(311). A change over between the two sets would be accomplished by a translation in the horizontal plane at right angles with the beam direction. The maximal beam width at the monochromator is approx. 50mm.

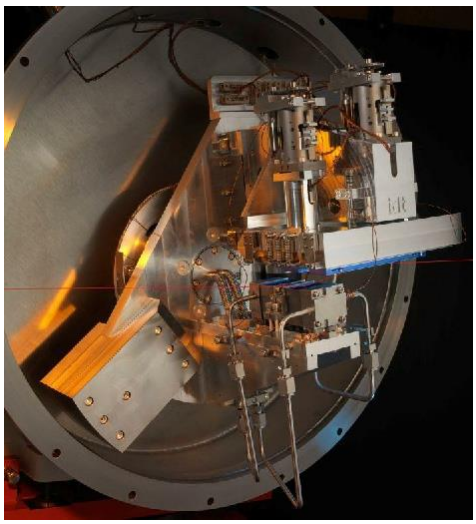

Figure 7: IDT dual crystal DCM installed at BM26A showing a side-by-side crystal arrangements and a long second crystal to allow for small Bragg angles.

For high energies, one would require either a long second crystal (200 mm) or an extra translation stage that moves the second crystal assembly. The gap between the crystals varies much less and a small stage with a range of 10 mm is more than sufficient.

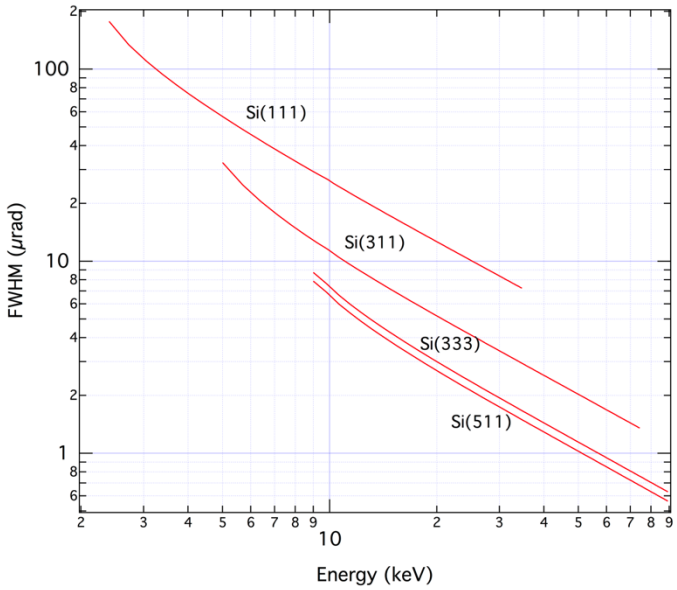

Figure 8: Angular Darwin width of a single Silicon crystal with different orientations.

An important aspect for spectroscopy is the energy resolution of the monochromatic radiation that is produced by the monochromator. With an Si(111) and Si(311) crystal available side by side in the DCM one has access to the Si(111), Si(311) and Si(333) reflections. The angular Darwin width (ζ) of each reflection is shown in figure 8 together with that of the Si (511) reflection for comparison. To cover the large energy range at least two different reflections must be used. For most cases is the Si(111) and Si(311) crystals suffice and give access to the full energy range of 2.4 - 62 keV. A Si(220) crystal set with a resolution between Si(111) and Si(311) was considered but the strong second harmonic would require frequent mirror adjustments.

The energy resolution can be found readily from figure 8 using the relationship:

$$\frac{\Delta E}{E} = \frac{\zeta}{\tan\theta}$$

The current monochromator has Si(111) and Si(311) which provide an energy resolution of $1.3x10^{-4}$ and $0.5x10^{-4}$ respectively. The photon energies available as a function of crystal reflection is shown in table 4.

E (keV)	Si(111)	Si(311)	Si(333)
2.1	70.3		
2.4	55.5		
3	41.2		
5	23.3	49.2	
7	16.4	32.7	
9	12.7	24.9	41.2
10	11.4	22.2	36.4
12	9.48	18.4	29.6
14	8.12	15.9	25.1
17	6.68	12.9	20.4
20	5.67	10.9	17.3
25	4.54	8.71	13.7
33	3.43	6.59	10.4
45		4.83	7.57
60		3.62	5.67
75			4.54
80			4.25

Table 4: Bragg angle in degrees for various DCM crystals versus photon energy

With the expected flux gain the new beamline will provide a higher flux using a Si(311) monochromator as compared to BM26A with a Si(111) monochromator using similar focusing and slit settings. One can also opt for Si(333) without changing crystals by filtering the first harmonic of the Si(111) reflection. For Si(333) the energy resolution is $0.3x10^{-4}$. The trade off for the higher energy resolution is a lower flux and the relative intensities of the different reflections are shown in table 5.

Crystal plane	Intensity	Energy Resolution (ΔE/E)
Si(111)	45.85	$1.26x10^{-4}$
Si(311)	20.74	$5.10x10^{-5}$
Si(333)	15.88	$2.90x10^{-5}$
Si(511)	14.3	$2.5x10^{-5}$

Table 5: Monochromator crystal choice – Intensity and energy resolution comparison

Please note that the above values reflect the intrinsic energy resolution that can only be achieved using a single crystal reflection and a beam that is vertically collimated. The vertical divergence of the source is generally much larger than the angular Darwin width. Even when a collimating mirror is used one has to consider the influence of the vertical source size. Consider the situation shown in figure 9 where the first (white beam) slits are almost closed.

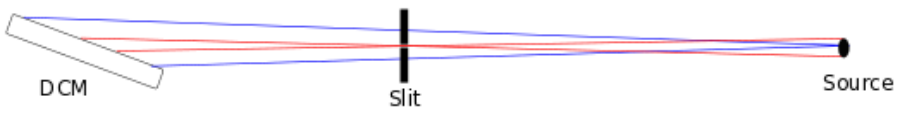

Figure 9: Vertical source divergence and size effects on energy resolution.

With a vertical source size of 0.004mm, the resulting vertical divergence for a small vertical gap of the white beam slits is 0.004 mm/30 m= 0.133 µrad. This is much smaller than any of the angular Darwin widths. The vertical source size is a feature of the machine lattice and is not dependent on the type of insertion device. Collecting a larger vertical fan of radiation results in a quick degradation of the energy resolution. For example, a 0.5 mm gap

of the white beam slits positioned at 30 m from a point source would result in a 16.6 µrad divergence (ψ), which is comparable with the intrinsic angular Darwin widths shown in figure 8. The above equation that expresses the energy resolution of the monochromator in combination with the source becomes:

$$\frac{\Delta E}{E} = \frac{\sqrt{\zeta^2 + \psi^2}}{\tan\theta}$$

To avoid beamline energy resolution degradation at higher flux (by increasing the vertical slit gap) we therefore need a collimating mirror, which is placed upstream from the monochromator.

The ESRF is engaging with an effort to improve the performance of DCM's in terms of stability. The best performing systems have a pointing stability of about 50-100 nrad. At a distance of 30 m from the monochromator these movements would result in beam changes that are significantly smaller than the beam size. Typical systems, however, perform significantly worse and one has to consider their effect on beam stability carefully. Especially for fast energy scanning applications. The best commercially available system reports an angular stability figure of 54 nrad and relies on an air bearing rotation axis (IDT Ltd.).

Traditional DCM systems feature relatively slow energy scanning speeds that make it impossible to collect complete scans within a few seconds make it hard to follow chemical reactions in situ. One of the key reasons why current scanning time is limited is the motor and drive system used to change the energy. By changing to a drirect driven axis (rather than the use of a mechanical gearing system) this problem is solved and the stability is also improved.

4.3.1 Heat load

In the worst case scenario (large Bragg angle, no collimating mirror) the first crystal is exposed to the white beam with a power density of 1.8 W/mm^2 with a total loading of more than 500 W (see figure 10). The lowest energies produced by the source are absorbed in the Be vacuum window. When use is made of the VCM to filter the white beam the total heat load on the monochromator is reduced to about 100 W (see section

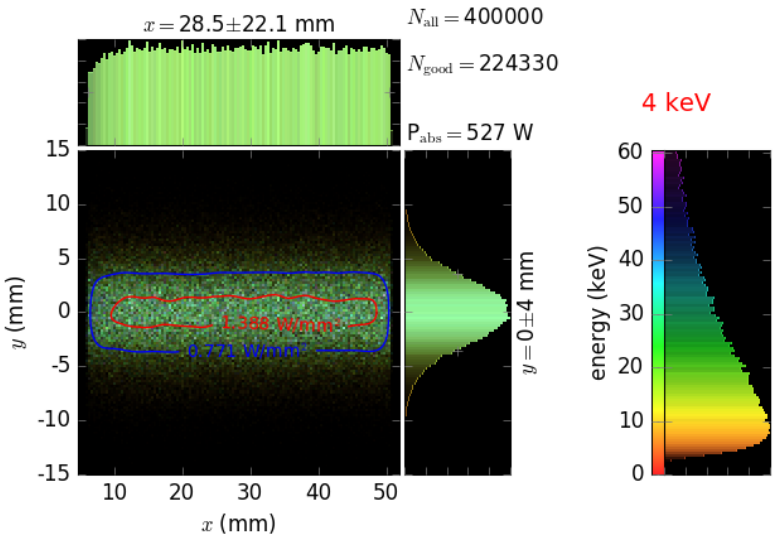

Figure 10: Worst-case scenario for first monochromator heat load as calculated by ray trace calculations performed at a DCM setting of 4 keV using the full available beam without collimating mirror. The incident spectrum is shown on the right. The total power absorbed by the crystal is shown as P_{abs}.

Given the fact that the angular Darwin width (or acceptance angle) of the Silicon crystals is of the order of micro-radians, we have to keep thermally induced distortions to a minimum. Requirements for cooling of the optical components that are exposed to the white beam are discussed in a separate section later in this document.

4.3.2 Energy Scans

The higher flux levels will allow faster scanning of the monochromator. The Bragg angle rotation speed is limited to max. 1°/s and it will not be possible to increase this significantly due to the large mass and sensitive nature of the components mounted on the common Bragg angle plate. For a higher temporal resolution one has to use a more compact monochromator design. The simplest option is to use a channel-cut monochromator and allow this to oscillate over a variable angle range. In the literature this technique is labelled with quick EXAFS or QEXAFS. A suitable approach to implement this technique is discussed later in this document.

Compared to the step-scan acquisition strategy it would be advisable to add a *continuous scan* operation mode. The integration of high-resolution encoders with hardware counters and advanced triggering systems that do not rely on slow software position readout will allow fast and smooth data acquisition [4]. Such a system would also allow data collection during energy scans in both directions avoiding idle time during which the monochromator is moving back to its starting position. Preparatory work regarding the implementation for this mode is already underway.

Motorisation of the DCM should include coarse and fine control over the pitch of the second crystal (DCM rocking curve tuning). Also second crystal roll and yaw should be adjustable (same as current IDT mono). A transverse motion to select between the two sets of crystal should also be available. In addition it is required to include a motorized DCM height axis to allow for different angles of incidence of the collimating mirror and changes of the white beam height. Currently the DCM height is not motorised, this should be changed such that the monochromator can be placed at the right height which is a function of the VCM incidence angle.

Recently, the exclusive use of in vacuum stages has been used to do away with a cumbersome vacuum feed through and differential pumping. This approach allows for more compact monochromators that should be more mechanically robust and stable. With the expected increase in brilliance careful consideration should be given to the vibration sensitivity of the mechanical setup. Especially the mount of the second crystal is critical due to the fact it relies on three motorised axes needed for alignment with respect to the first crystal. Good engineering practice should be able to avoid any major resonance peaks in the frequency spectrum. Ideally rotating machinery such as vacuum pumps will be removed from the vicinity of the monochromator.

Adding a quick scanning channel-cut monochromator(s) will be relatively easy as long as some space is reserved to place a relatively small vacuum vessel upstream or downstream of the DCM. Such devices could act as pre- or post DCM monochromators to tailor the energy bandwidth or used separately for fast scanning applications. It would be possible to use a pair of channel-cut monochromators to create a ‘two-colour’ beam that would be of interest in compound or bi-metallic studies.

4.4 Focusing Optics

4.4.1 Toroidal Mirror

➔ *A 2:1 toroidal focusing mirror (TFM) is chosen which is mechanically bent in the shape of a cylinder to provide a focal spot at the sample position. The mirror has coated flats on either side of the cylindrically shaped groove to allow for vertical focusing only options at various angles of incidence and sample positions.*

The collimated and monochromatic beam emanating from the monochromator is rather large and further optics is required to focus the beam at the sample position. Several schemes can be employed to do so, each with specific issues that merit some discussion. One alternative that uses a sagittal focusing monochromator is not appropriate because of the reduced energy resolution of this solution. Separating horizontal and vertical focusing elements using two orthogonally placed mirrors is problematic due to the large horizontal extend of the radiation fan.

Toroidal mirrors are convenient from a point of operation. By bending a long toroidal mirror a finely focused beam is obtained at the sample position. The choice for a toroidal mirror fixes the position of the sample and the angle of incidence that should be used. Use of the toroidal mirror at different than the design angle will lead to defocusing which could be beneficial if a larger sample area must be probed.

There are several situations where a fixed sample position and the use of horizontal focusing would be problematic. For example, when dealing with larger samples a user might prefer to probe a larger area with a bigger beam. The requirement for a fixed sample location can also be problematic with larger sample environments or in experiments with combined small angle scattering setups where the focal spot would be preferred to lie at the detector position.

Typically the meridional curvature is large and the sagittal curvature is small as described by:

$$R_s = 2 \sin\alpha \left(\frac{pq}{p+q}\right)$$

$$R_m = 2\, q \sin^{-1}\alpha$$

Here *p* is the source to mirror distance and *q* is the mirror to focal spot distance. For the case of a 2:1 demagnification and a 2.4 mrad angle of incidence we find R_s = 54 mm. For the meridional radius of curvature we get a value of R_m = 14 km with collimating mirror or 9.4 km without one. As shown by MacDowell *et al.* [5] the optical system consisting of collimating mirror and toroidal focusing mirror with a 2:1 horizontal demagnification has the benefit of eliminating astigmatic coma. With the toroidal mirror at a distance of 34 m from the source the sample position is fixed at 51 m.

To provide the user with a more flexible arrangement it is proposed to provide a combined flat and toroidal mirror that has a cross section with a toroidal central section (Pt-coated) and two flats to either side that are coated with different materials (Si, Rh) to allow for a wide energy range (see figure 12).

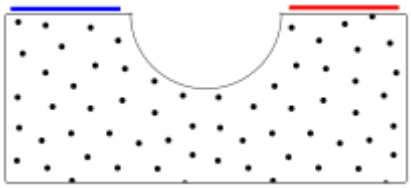

Figure 12: Cross section of proposed toroidal mirror (not to scale). Blue and red surfaces indicate different surface coatings for the vertical only focusing areas of the mirror.

By horizontal movement, one of the three surfaces can be selected giving the user a wide choice in cut-off energy and focusing conditions. In order to capture most of the vertical extend of the beam a mirror of about 1.2 m long would be used with a width of 100 mm. The toroidal part would only cover about 50-60 mm leaving two flat sections of 20 mm in width. Such a mirror would be identical in size as the current flat mirror allowing its vacuum vessel and translation stages to be reused.

The RMS profile error of the polished mirrors should follow the Marechal criterion taking into account that there are N reflections (min. are two mirrors and two monochromator crystals) and that the mirror is exposed at a grazing angle:

$$\sigma \leq \frac{\lambda}{14\sqrt{N}2\alpha}$$

With four reflecting surfaces, a grazing incidence angle of 3 mrad and a design wavelength of less than 0.1 nm, the RMS profile error should be smaller than 0.6 nm.

A single toroidal mirror fixed at an incidence angle of 4.5 mrad will cover a wide range of energies up to about 20 keV (see table 6).

Photon Energy	TFM coating	VCM coating	Angle (mrad)	Note
2.4 – 7 keV	Pt	Si	4.5	-
-	Si	Si	4.5	Only Vert. focusing
7 – 20 keV	Pt	Pt	4.5	-
-	Rh	Pt	4.5	Cut-off 15 keV
-	Rh	Rh	3.3	Only Vert. focusing
20 – 35 keV*	Pt	Pt	2	-
35 – 62 keV	-	-	-	No mirrors

*** By reducing the mirror angle to 1.6mrad this range can be extended to 50 keV**

Table 6: Mirror coating combinations and mirror incidence angles for the three energy ranges. The toroidal part is coated with Pt. If no Pt is chosen the user can still decide to focus the beam vertically but not horizontally (similar to current situation at BM26A).

Due to the significant source size reduction the quality of the mirrors used becomes a very important parameter. Particularly the size of the vertical focus that can be obtained is a function of the RMS slope error of the mirror. To preserve the small source size it is important to study the effect of slope error on focal spot size. To this end we have performed ray trace calculations with mirrors of varying slope error to avoid introducing significant losses in source brilliance. In order to perform realistic simulations of beamline performance we have contrasted perfect mirrors with real mirrors that have roughness and slope errors. To focus the 2PW source without significant distortions mirror slope errors must be smaller than the angular size of the source or 4/34 = 0.1 µrad.

Unfortunately this figure is difficult to achieve for a mirror of sufficient length. For mirrors with RMS slope errors of 0.65 µrad[i], preliminary ray trace calculations with XRT result in a 70 x 140 (*hxv*) µm^2 FWHM spot size (see figure 13). This calculation was performed for an energy of 12 keV without VCM inserted into the beamline providing a worst-case scenario.

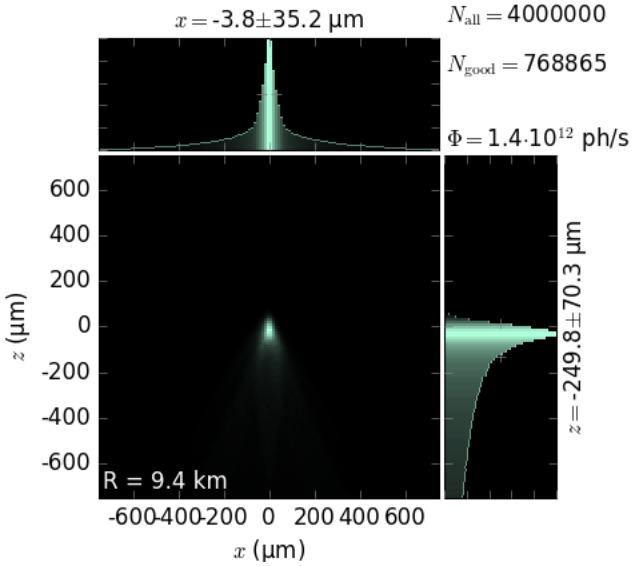

Figure 13: Ray trace calculations for the toroidal mirror in the 2:1 geometry without VCM. An RMS slope error of 0.65 µrad of the mirror is used in the calculations.

Even for a perfect toroidal mirror we are *unable* to resolve the two transversally separated source points of the 2PW insertion device, which is encouraging. In the calculations we have aligned all components perfectly. Angular alignment with the 2PW insertion device is more critical than compared to a traditional (multi-pole) insertion device. For example, a 0.8 mrad misalignment would give maximum separation between the two magnet poles and a ray trace calculation (figure 15) clearly shows the two contributions separated at the sample position. Conversely, a small rotation in the opposite direction would bring both poles inline with each other resulting in the smallest source size.

ⓘ *The long tails of the intensity distribution are typical for mirrors that use a cylindrical approximation of what ideally should be an ellipsoidal mirror. Use of a double moment bender system would eliminate this artefact.*

❖ *For comparison, we have re-run the ray trace calculation for a perfect mirror and find a spot FWHM of 70 x 60 (hxv) µm² indicative that the vertical dimension of the focal spot is very sensitive to slope errors.*

For the B option of the 2PW, the closest dipole (DQ1D) radiation fan overlaps with that of the 2PW but due to a small angular offset these two sources are transversally separated at the sample (see figures 14&15). Using secondary slits close to the sample the dipole contribution can be cut away.

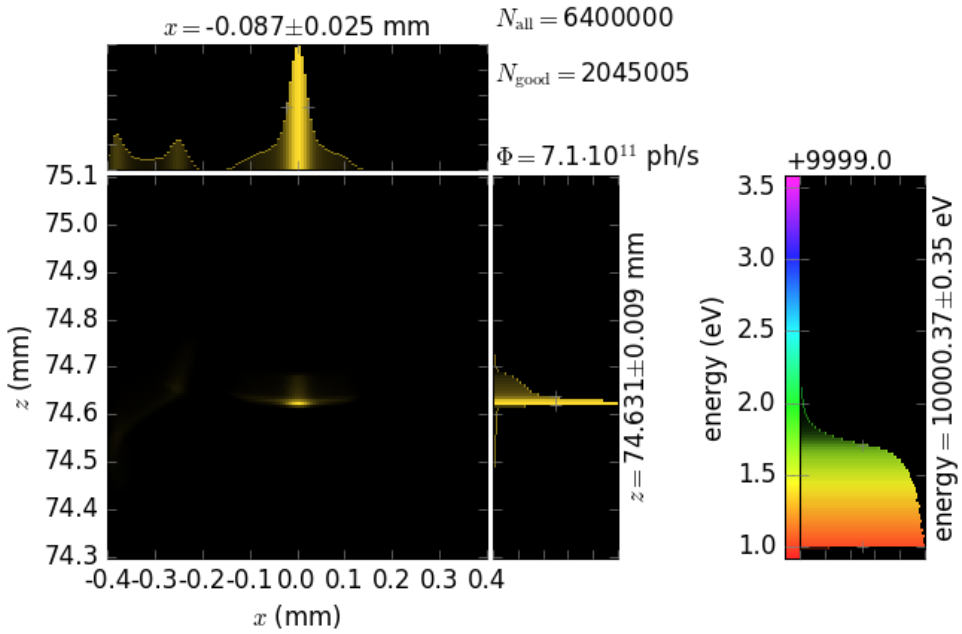

Figure 14: Ray trace calculations for the toroidal mirror in the 2:1 geometry with VCM for 10 keV radiation with both mirrors at an angle of 4.5 mrad. Mirrors were taken to be perfect and aligned centrally along the 2PW-B axis. The side peaks to the left of the main peak are due to the downstream DQ1D dipole.

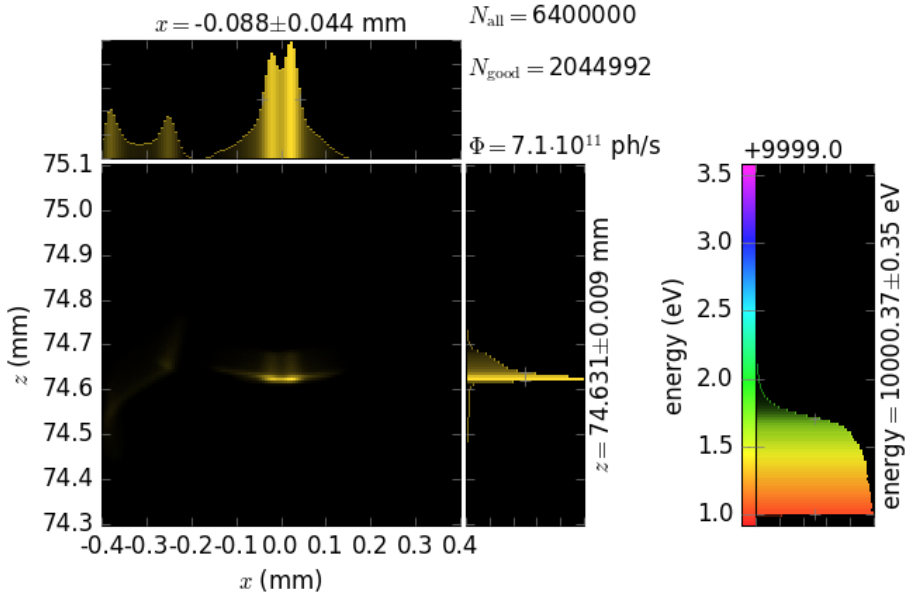

Figure 15: Ray trace results for 10 keV photons with alignment at 0.8 mrad away from the central 2PW-B axis. Ray trace calculations for the toroidal mirror in the 2:1 geometry with VCM for 10 keV radiation with both mirrors at an angle of 4.5 mrad. Mirrors were taken to be perfect. For this angular shift both wiggler poles are just resolved.

4.4.2 Kirkpatrick-Baez mirror system

The Kirkpatrick-Baez (KB) focusing mirrors are non-chromatic and are therefore ideal for energy scanning applications and will operate over the full beamline energy range using two metal coating stripes if necessary. Using a relatively large demagnification (as compared to that of the toroidal mirror) this device allows a significant reduction in focal spot size that is required by experiments that require high spatial resolution spectroscopy measurements. The device will be fully integrated into the beamline design and motorised such that it can be remotely inserted into the beam path. The geometry of a KB mirror produces a finely focused beam, which is both laterally and vertically shifted compared to the incoming beam path. This shift, however, will typically be of the order of 10 mm and should be within the range of sample positioning equipment.

KB mirrors operate with a high demagnification ratio of 100:1 or higher; as a consequence they are placed close to the sample - typically at a distance of 0.2 - 1 m. For the spectroscopy beamline with the sample at approximately 51 m from the source a demagnification ratio of up to 250:1 is possible. DUBBLE has recently taken ownership of a System-I KB mirror system from the ESRF optics group. This focusing optics is able to collect a 0.2x0.5 mm^2 (*hxv*) section of radiation when operating at a 3.5 mrad angle of incidence. The mirrors have a coating of Rh resulting in an energy cut-off of 18 keV.

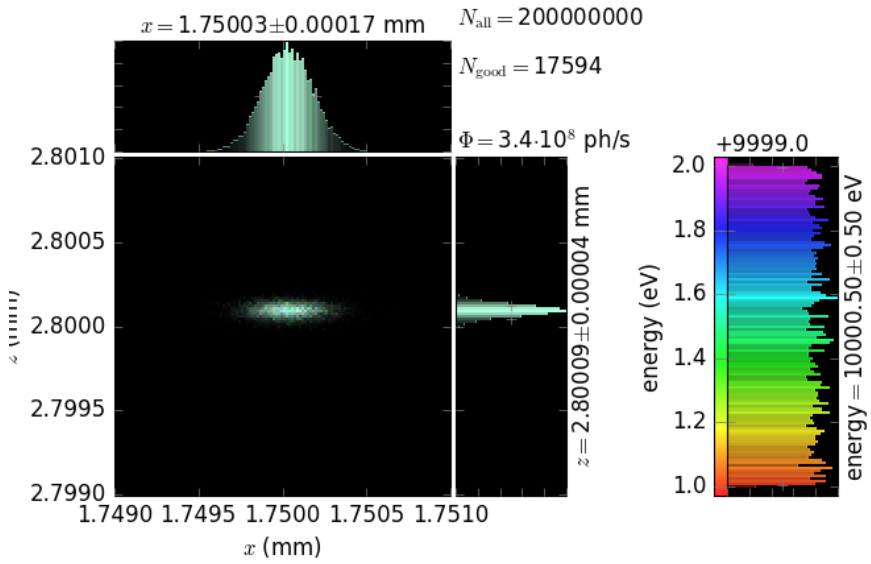

Figure 16: Ray trace results for an ideal KB System I mirror system placed close to the sample, which is located at 51 m from source using 10 keV photons. In the calculations the full 0.2x0.5 mm² aperture of the KB system was filled.

Due to the short sample to KB mirror distance, this setup would be placed in the experiments hutch. Because the horizontal size of the beam is larger than the vertical one the horizontal focusing mirror should be the one closest to the sample allowing a higher demagnification than for the vertical direction.

The calculations were performed with and without the DQ1Q source showing no difference in the focal spot other than a slightly reduced flux at the sample for the case without the dipole contribution. Due to the high demagnification the focal spots of the side dipole and wiggler poles merge into a single sub micrometre-sized spot.

☒ *The example KB system used has a rather modest acceptance and KB mirror systems with a larger acceptance could be used to increase the flux albeit at a slightly larger focal spot size but this would need further investigation.*

❖ *According to the simulations the System I KB system will deliver 3x10^8 photons/s with an energy of 10 keV into a 0.3x0.1 µm^2 (hxv) focal spot.*

Other types of KB mirror systems could be considered that feature larger acceptance angles or have the sample closer to the exit of the mirrors with the aim of increasing photon flux or decreasing spot size. Whatever system is chosen it will have to be placed close to the sample and located in the experiments hutch.

4.5 Optics Modes

In this section the various modes in which the x-ray optics can be used will be discussed. Due to the choice of mirror optics several modes may be selected depending on the required beam size, energy resolution and selection of large coherent fraction. The options combined provide a rich selection of beamline setups that will cater for a wide variety of experiments in addition to standard spectroscopy setups that don't necessarily require a tightly focused beam. Due to the presence of flat sections on the surface of the toroidal mirrors it is still possible to deliver an unfocused beam at the sample position allowing the highest energy resolution possible. The preferred optical setup does offer a variety of measurements options providing for a wide range of experiments.

- Large coherent fraction/Unfocused, aperture limited
- High flux, doubly focused using toroidal mirror
- Direct KB focused - small focal spot
- Compound focusing for full field imaging
- (Optional) High energy focused Laue (>50keV)

Main guide to the above focusing scenarios are given by the following guidelines regarding the experiments of interest:

- If the phase-space acceptance of the experiment is smaller than the phase-space area of the X-ray beam in the plane then X-rays must be lost (similarly in y). In this case we say it is a brightness experiment
- If the acceptance of the experiment is greater than the beam emittance then 100% of the beam can be accepted - this is a flux experiment
- If the acceptance of the experiment is for a beam of phase-space area $\lambda/2$ then this is a coherence experiment and for current storage rings light is always lost

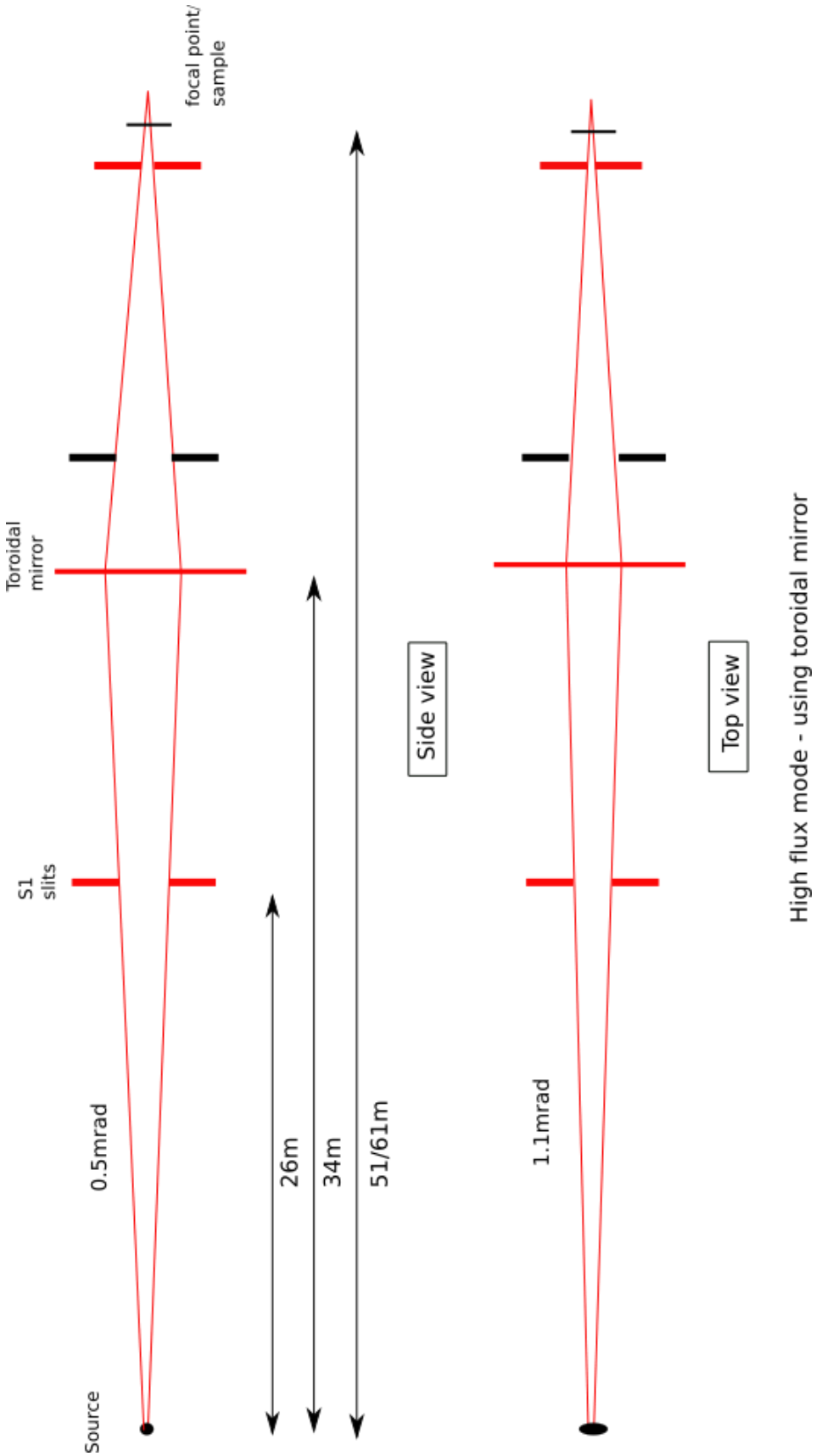
focal point/
sample
Toroidal
mirror
S1
slits
0.5mrad
Source
26m
34m
51/61m
Side view
1.1mrad
Top view
High flux mode - using toroidal mirror

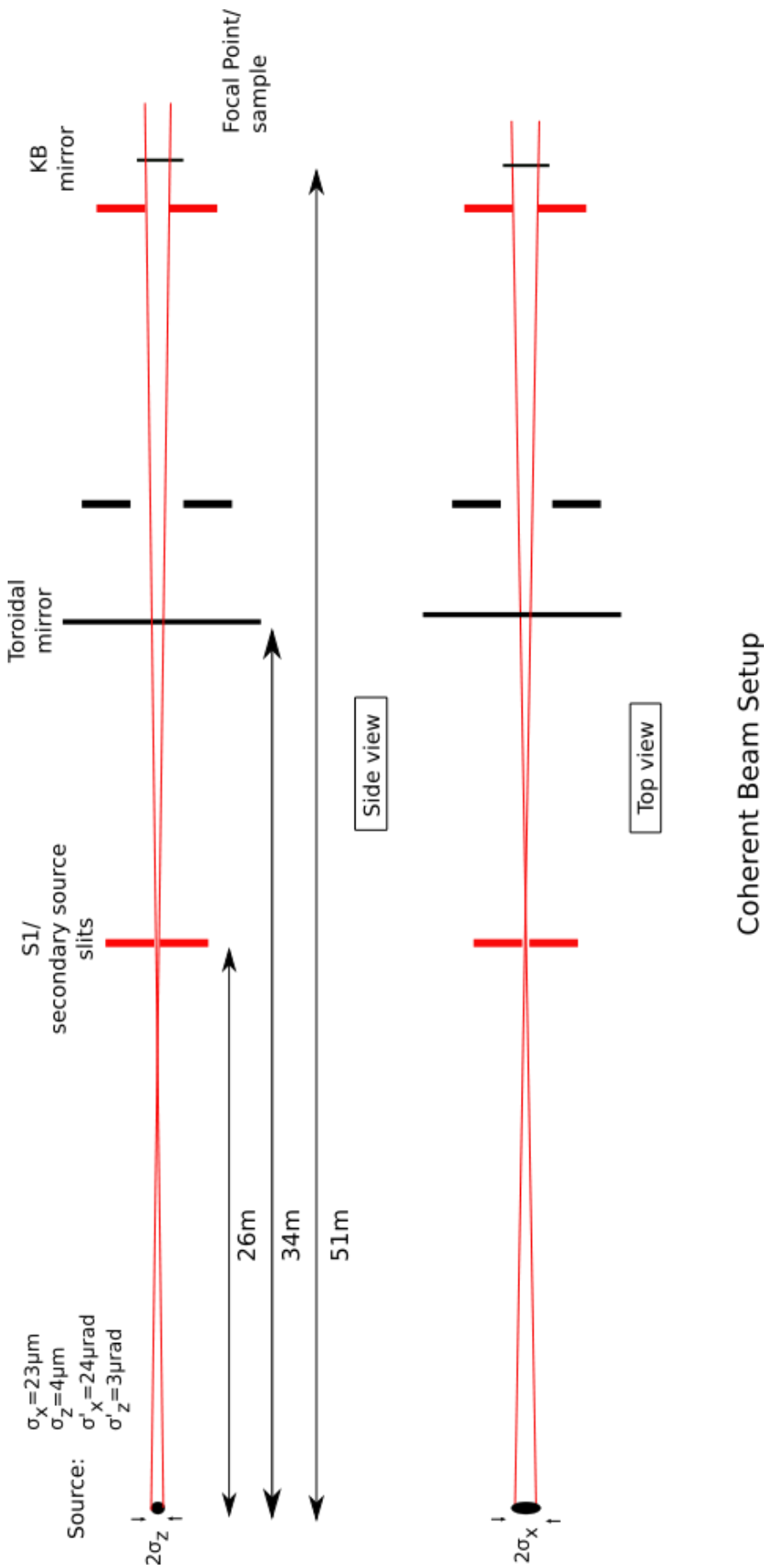
Coherent Beam Setup
Side view
Top view
KB mirror
Focal Point/ sample
Toroidal mirror
S1/ secondary source slits
Source:
σx=23µm
σz=4µm
σ'x=24µrad
σ'z=3µrad
2σz
2σx
26m
34m
51m

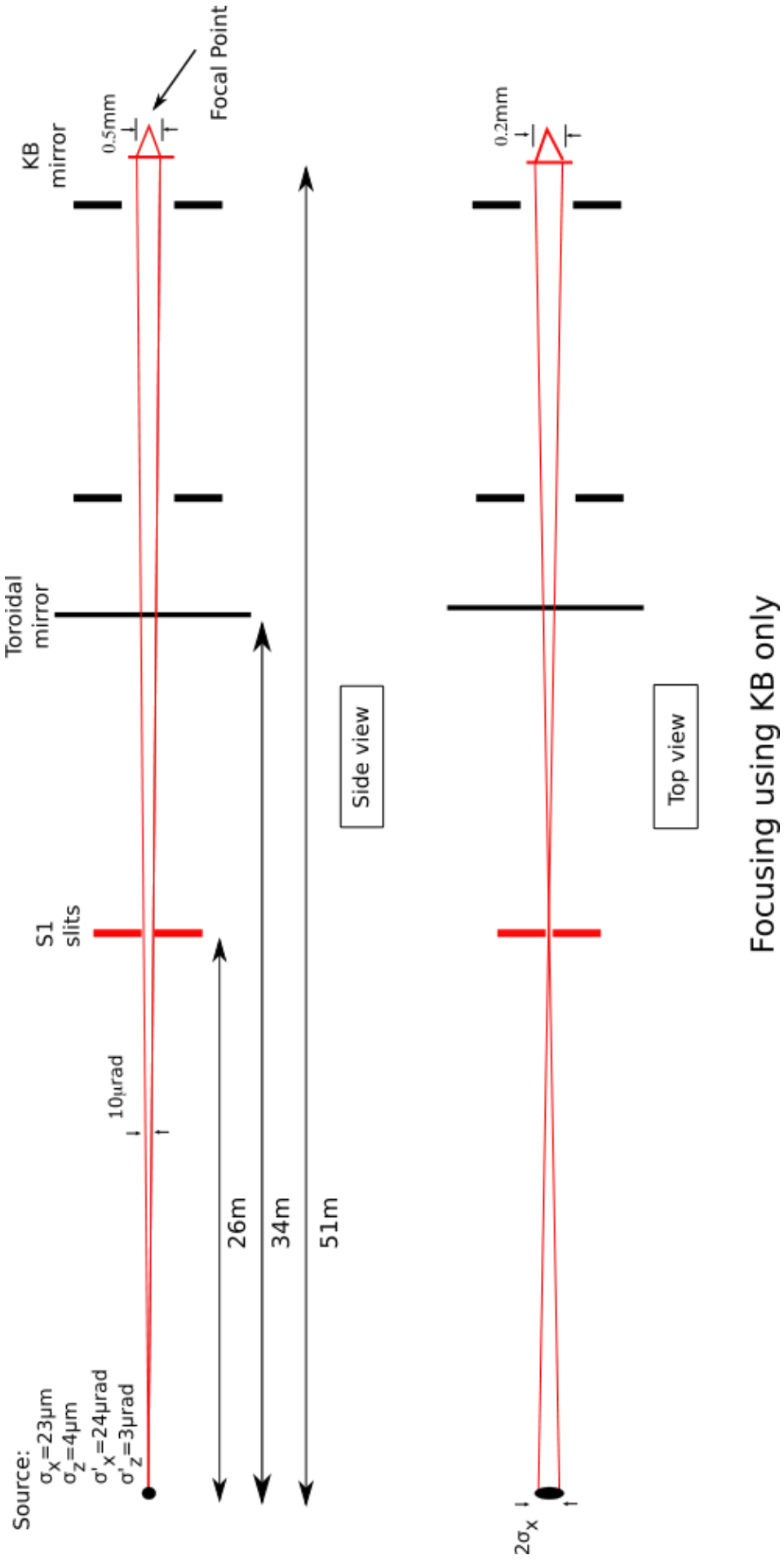
Focusing using KB only
Side view
Top view
KB mirror
0.5mm
Focal Point
Toroidal mirror
S1 slits
10μrad
26m
34m
51m
Source:
σx=23μm
σz=4μm
σ'x=24μrad
σ'z=3μrad
0.2mm
2σx

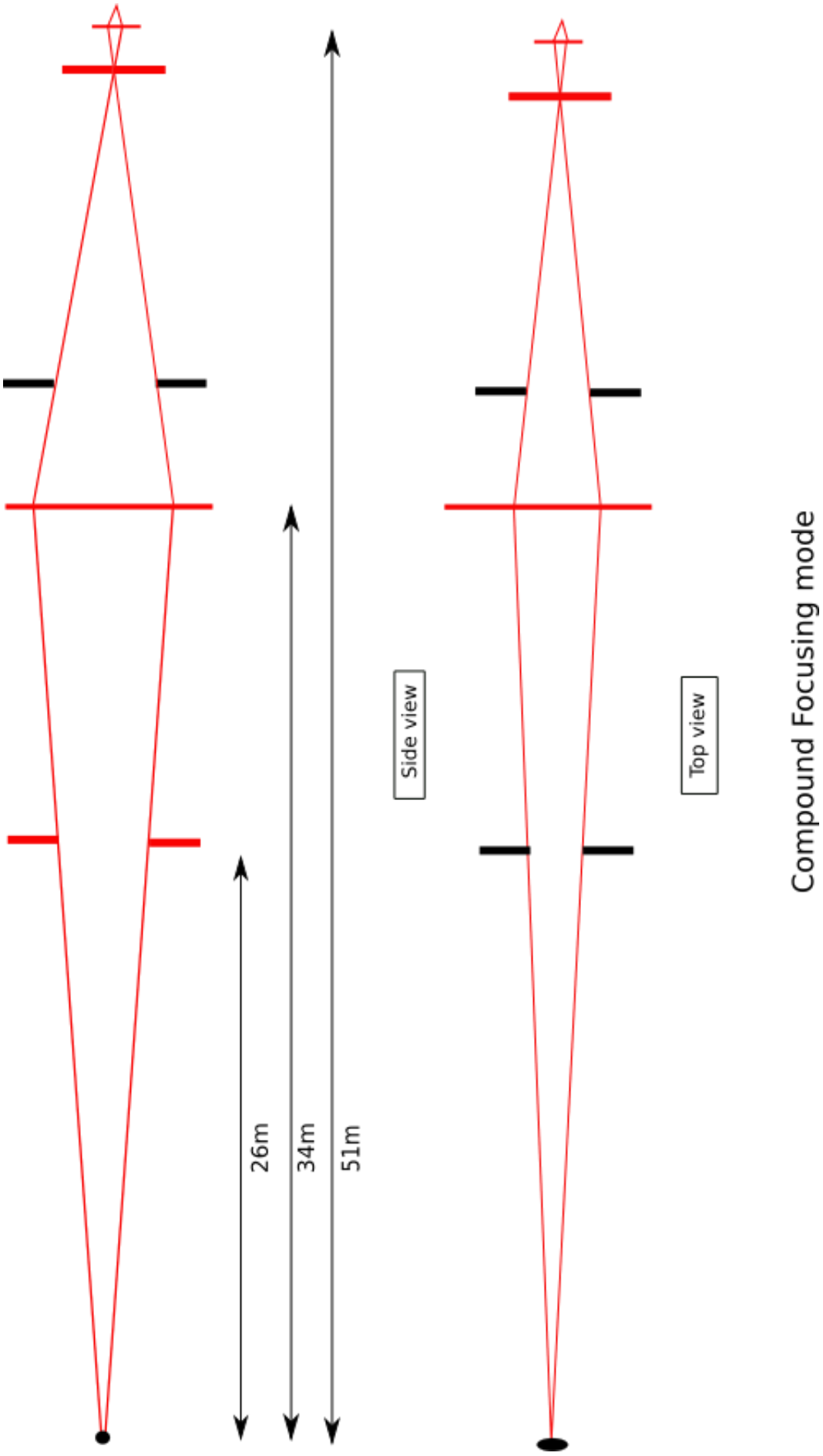
Compound Focusing mode
Side view
Top view
26m
34m
51m

4.6 Comparison with existing BM26A facility

A ray trace study was performed for the existing BM26A facility, which receives radiation from a 0.4T bending magnet. In the study, we have included the expected performance of the proposed facility providing a side-by-side comparison using settings that are often used during actual experiments. The demagnification ratio at BM26A is 5.5 compared to 2 for the proposed beamline. The data for the proposed beamline have been calculated without horizontal focusing (BM26A has no provision for focusing the beam horizontally) using an identical horizontal and vertical acceptance for a fair comparison. The ray trace calculations were performed using mirrors with a RMS slope error of 1.65 µrad. Mirrors are set at a 2 mrad angle of incidence and have a Platinum coating. BM26A measured flux was only available for a vertical gap of 1 mm, which seems to correspond fairly well with the ray trace result.

	BM26A				Proposed	
First Slit vertical gap (mm)	Vertical Acceptance (mrad)	Measured: vertical Beam size FWHM (mm)	Measured: flux at sample (ph/s)	Ray trace: flux at sample (ph/s)	Flux at sample (ph/s)	Vertical beam size FWHM (mm)
0.5	0.0208	0.3	-	$1.5x10^{10}$	$3.5x10^{10}$	0.27
1.0	0.0416	0.65	$2x10^{10}$	$2.9x10^{10}$	$7.1x10^{10}$	0.27
1.5	0.0625	1.0	-	$4.3x10^{10}$	$1.1x10^{11}$	0.28

Table 7: Comparison between the existing beamline BM26A and the proposed upgrade for a photon energy of 12 keV. Measured values are listed when available. The measured vertical beam sizes are larger than expected for the demagnification factor used, even when a significant slope error of the mirrors is used.

Slits are used to accept 0.1 mrad horizontally proving a horizontal beam size at the sample of about 4 mm width. Data from BM26A is available for three vertical slit settings as shown in table 7. The comparison is made at a photon energy of 12 keV.

Energy (keV)	BM26A	Proposed
8	$2.7x10^{10}$	$5.9x10^{10}$
12	$2.9x10^{10}$	$7.1x10^{10}$
26	$1.2x10^{10}$	$5x10^{10}$

Table 8: Comparison between the existing beamline BM26A and the proposed upgrade for three photon energies which span de range of the Si(111) monochromator. The calculation was done for a vertical slit gap of 1 mm.

Table 8 captures the calculated intensities at three energies, showing the fact that the 2PW source provides a spectrum shifted to higher photon energies compared to that of BM26A.

The measured vertical beam size at BM26A is unexplained; based upon the ray trace calculations a vertical FWHM beam size of about 0.1 mm is to be expected. Increasing the mirror slope error beyond a value of 1.65 µrad doesn't explain the measured value. This anomaly is probably due to a mirror bending issue.

As expected, the biggest gains are made when the beam is fully focused. Use the same settings as above for the horizontal acceptance of 0.416 mrad we perform ray trace calculations at 12 keV using mirrors with three different slope errors to gain insight into how slope errors affect focal spot size (see table 9).

RMS slope error (µrad)	Horizontal FWHM (mm)	Vertical FWHM (mm)
0.33	0.04	0.05
0.5	0.04	0.08
0.67	0.05	0.12
1.65	0.05	0.27

Table 9: Relationship between mirror slope error and focal spot size at the sample for the proposed beamline. BM26A mirrors are specified as having a 1.5 µrad RMS slope error.

Commercial suppliers of x-ray mirrors list their capability for long mirrors (> 1m) with RMS slope errors of 0.1 µrad (J-TEC) or 0.2 µrad (SESO). These specifications, however, will be very expensive. Judging from the results listed in table 8 it seems beneficial to aim for an RMS slope error of 0.5 µrad or better. A careful cost versus benefit analysis will be required.

Equally important is the quality of the mirror bender. For the collimating mirror the radius of curvature is large and adjustment must be made for gravity sagging of the mirror. Fortunately good commercial solutions are available. From the figures above it seems obvious that BM26A has an issue with one (or both) of the mirror benders. Without solving this issue the above investigation into slope errors seems futile.

An interesting development by SESO regarding a new concept of a long uniform bimorph mirror should be considered as an option for the focusing mirror. In either case good beam diagnostics will be required to adjust mirror bending/shaping. In the case of multiple piezo actuators

The true benefit of the proposed upgrade becomes clear when working with the doubly focused beam, which is able to deliver $7x10^{10}$ photon/s into a focal spot of 40 x 230 (or better) μm^2. *Compared to the flux density from BM26A this represents a 1000-fold increase!*

Increasing the solid angle of radiation transmitted by the first set of slits will allow users to increase the flux of 12 keV photons at the sample to about $1.4x10^{12}$ photons/s as listed earlier. Please note that this value is limited by the acceptance of the mirrors and monochromator.

4.7 Filters

The use of a water-cooled filter rack is very helpful in various circumstances and a relatively simple device to install. Together with the use of x-ray mirrors with different coatings a very effective energy filter is realised that helps to keep heat load on optical components down and reduces higher harmonics from reaching the sample. Ideally the filters are made of different materials and thicknesses so that the beam can be attenuated by well-known factors. Materials suitable for filters include: Aluminium, graphite, glassy graphite (Sigradur K & G – www.htw-germany.com), CVD diamond (www.cvd-diamond.com).

Figure 17 shows the available flux as a function of energy for different combinations of mirrors (all at 4.5 mrad) and/or filters in order to limit the transmitted spectrum. For all calculations we used aperture size of $1x0.1\ mrad^2$ (*hxv*). Please note that only a single mirror reflection was used in the calculations.

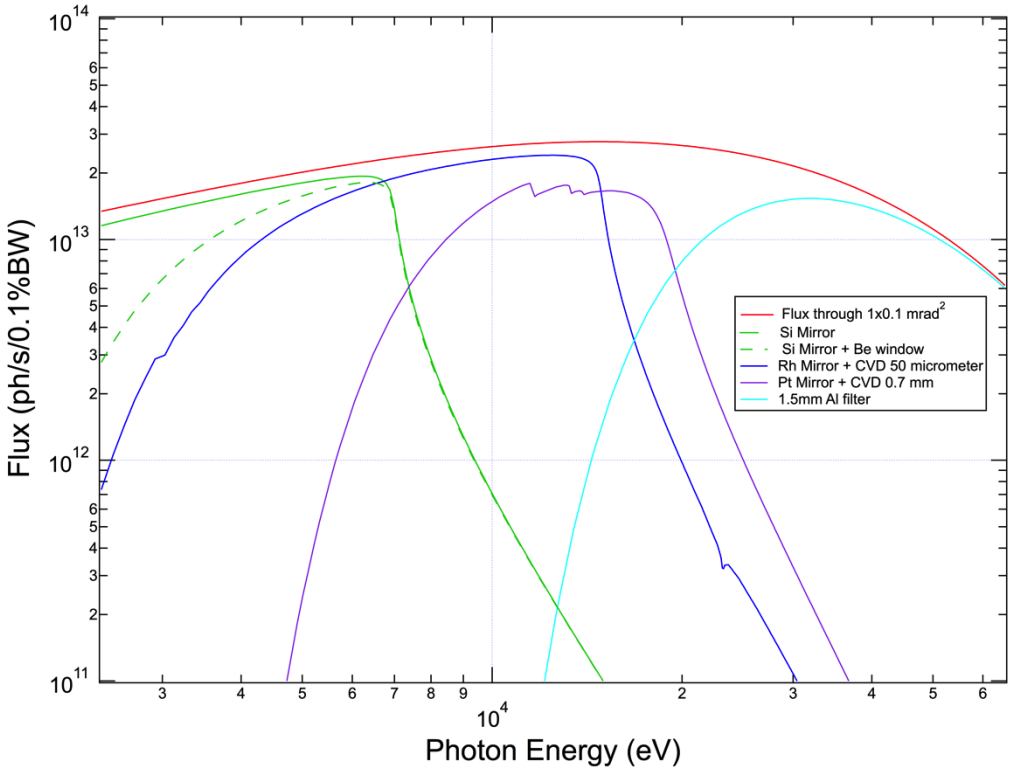

Figure 17: Expected flux at the sample for a white beam aperture of 1x0.1 mrad2. Various filters and mirror coating combinations can be used to filter away particular energy ranges, which is helpful for reducing harmonics and heat loading. Only a single mirror reflection was used in the calculation and the angle of incidence was 4.5 mrad for all cases.

Optional are higher-Z elements such as Tungsten.

➔ *It is proposed to have two motorised racks with four to five slots that contain all the filters in a water-cooled support in a location upstream of the collimating mirror.*

Particular for the high-energy side of the spectrum in which the mirrors become less useful the filters take on the job of reducing the heat load on the monochromator effectively. Also for alignment purposes the ability to reduce beam intensity for the lower end of the spectrum is helpful.

4.8 Additional Optical Components

A beamline is only as good as its optical components. With the move to a new optics hutch of similar size as the current one (which holds optics for both BM26A & B) there is space available for future beamline upgrades. By embracing a forward looking stance in the initial design and placement of beamline vacuum components, upgrades can be made quick and simple if and when needed.

The following additional optical components can easily be accommodated in the new setup and would extend the functionality of the beamline.

- Focusing Laue monochromator (for photon energies > 50 keV)
- Type IIa diamond phase plates to vary and control polarisation
- Mirror/Grating combination for very low energies (500 – 3000 eV)
- Multilayer pre-monochromator (2% BW)/poly-chromator
- Additional toroidal mirror with Rh coating for low-energy point focusing
- Flat double mirror system for additional harmonics attenuation.

5. Cooling of optical components

The optical elements exposed directly to the white beam need cooling to preserve the brilliance of the source. The total flux is roughly a factor of 2 higher compared to the current situation and is concentrated in a horizontal fan that is slightly narrower than before (1.7 vs. 2 mrad) resulting in a total flux of about 800 W when integrated over all photon energies (and adjacent sources). By employing the right combination of collimating mirror coating and angle of incidence unwanted higher photon energies could be removed (see figure 17) when the beamline is setup to select low photon energies, whereas filters can be helpful to cut lower energetic photon in the opposite case. We have performed some examples of expected power loading which correspond to some extreme examples in which the loading of the monochromator is particularly high. Once thermal distortions lead to slope errors equal to a significant fraction of the crystal acceptance angle a significant reduction in monochromatic flux levels will be evident. Whilst it is unavoidable to have temperature differences a good cooling scheme can minimise these. Typically direct water-cooling can be used at a power density of up to approx. 1 W/mm^2. From figure 3 we can see that the new source delivers higher power densities than this threshold, which prompts the requirement for a careful look at the effects of beam heating on the monochromator in particular.

The alternative to water-cooling is to use liquid nitrogen (or cold He gas) and this has been used on undulator beamlines successfully for many years. Although liquid nitrogen has a lower specific heat compared to water this type of cooling works well due to the fact that Silicon crystals show no thermal expansion at temperatures near that of liquid nitrogen thus completely eliminating any thermal distortions even in the presence of significant power loadings. The relatively low power loading from the 2PW should allow a relatively simple indirect cooling scheme.

The existing monochromator cooling scheme uses an efficient direct water-cooling in which water flows through the monochromator crystal close to the diffracting surface using a relative simple setup. Based on this existing scheme for cooling the first monochromator crystal we will now assess its performance with the new source.

Although the whole area of the beam facing side of the first monochromator can be exposed to the beam, only a central subsection is in close contact with the cooling water. By exposing the whole (top) surface with a uniform power loading of 100 W in a finite element study one readily establishes the area of the crystal face that is cooled most effectively (see figure 18).

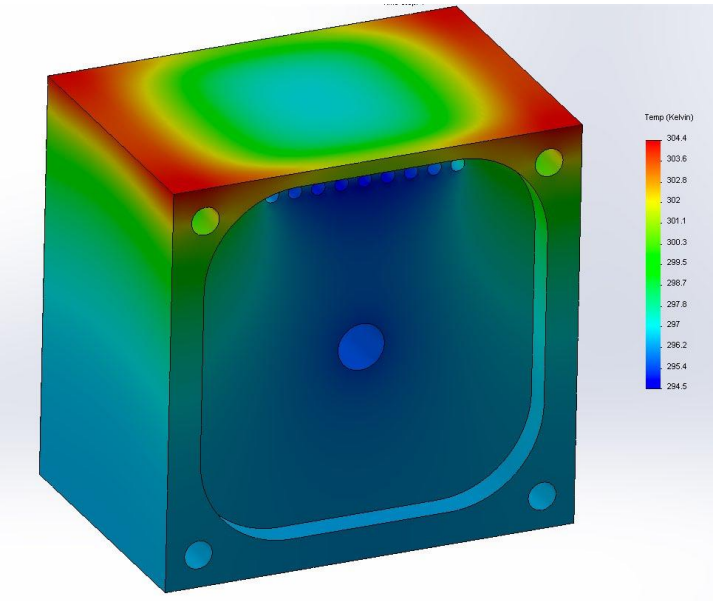

Figure 18: Monochromator crystal heat load study results. The top face is exposed to a uniform heat load of 100 W. The resulting temperature profile of the crystal shows a maximum temperature that is raised about 10 °C with respect to the water temperature for areas furthest away from the water-cooling channels. A central area of the crystal of about 20x15 (*hxv*) mm^2 is most effectively cooled.

Cooling is used in the model by passing water through the internal, wetted surfaces of the 9 bore holes and central return bore hole. The coolant is at a temperature of 22 °C. For a water flow rate of 4 litre/min, a heat transfer coefficient of 35237 W/m^{2}K is applied to the 9 small-bore holes and 10531 W/m^{2}K is used for the central hole which has a cross section equal in area compared the sum of the 9 small bore holes.

With the IDT crystal dimensions we should be able to accept 0.64 mrad horizontally (approx. 40%). Vertical acceptance of the monochromator is a function of Bragg angle and varies between 100% and 20% depending on the selected photon energy.

In assessing the effects of beam-induced heating we don't have to study every combination of mirror, slit and monochromator setting, it suffices to look at some cases in which the heat load and/or heat load density is largest. This would be for the larger Bragg angles such as reached at low photon energy. Fortunately, the collimating mirror acts as a very effective filter to remove most of the power from the reflected beam.

In our calculations, we use the current horizontal acceptance limitation of 0.64 mrad as set by the effective width (20 mm) of the first crystal of the IDT monochromator. If required, a wider crystal could be used to capture a larger fraction of the available horizontal divergence.

During the finite element (FE) calculations the power loading is applied to the crystal surface *only* whereas in reality power loading has a depth profile which increases in range when going to higher energy. Thus our calculations will therefore represent a worst-case scenario, which fulfils the purpose of our study. A uniform power distribution over the active area was applied which is a good approximation for most cases where the source divergence is cut down using slits.

Using appropriate combinations of filters, suitable angle of incidence of collimating mirror and coating of this mirror, one can limit first monochromator crystal heat load significantly (see figure 19) without compromising monochromatic flux.

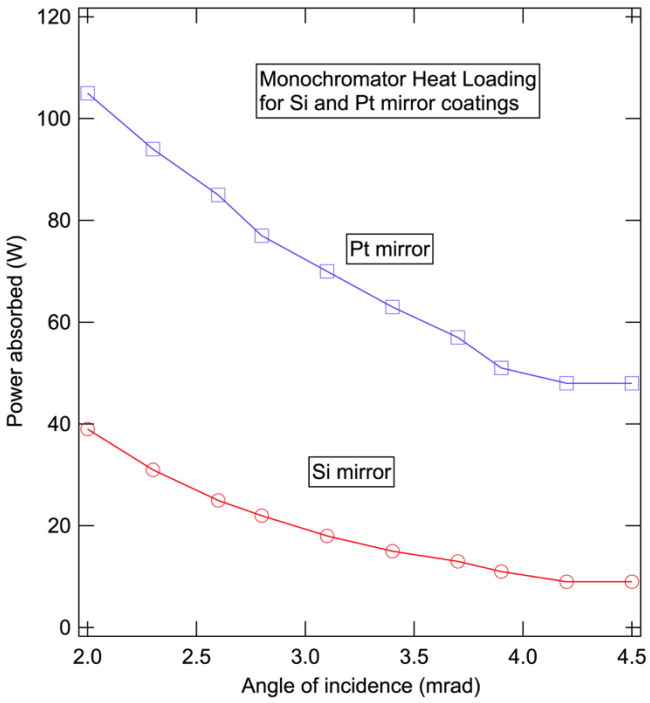

Figure 19: By selecting an appropriate mirror coating and angle of incidence effective heat loading of the first monochromator crystal can be controlled effectively resulting in a significant reduction. For 2.4 keV the variation of the heat load is particularly large (from 105W to 9W). A 0.64 x 0.12 mrad^2 fan of radiation is used in the calculation (limited by the monochromator crystal size).

For heat loads representing the highest expected heat load (105 W, 1.3 W/mm^2, the FE calculations predict a 35 µrad slope error which is about 1/3 of the Si(111) acceptance at 2.4 keV (see figure 8). For 10 keV this slope error is larger than the acceptance of the second crystal (see figure 20). Thus exposing the first monochromator crystals to this heat load (density) will result in a significant beam loss (and increase of beam divergence) which in the case of 10 keV would be unacceptably high.

For the case of 15 keV, the mirror with a Si-coating can't be used for incidence angles of more than about 2 mrad resulting in a lowest heat load for the monochromator of 40 W resulting in significant slope errors (see figure 20). At this energy users would have to reduce the vertical acceptance to mitigate beam heating issues. For 2.4 keV, the reduction achieved is over an order of magnitude resulting in a small loading of 9 W.

Finally, for high photon energies the crystal acceptance becomes rather small and heat 'filtering' with collimating mirror angle and coating becomes less efficient. For such cases filters should be used to remove lower photon energies and some examples in which lower energies are effectively removed are shown in figure 16. For these high energies the power absorption is also distributed deeper into the crystal allowing a far more efficient removal of heat. Nevertheless, for higher energies the angular Darwin width decreases rapidly (see figure 8) to the point that the smallest thermal distortion results in a significant loss of flux (50%) at a photon energy of 30 keV.

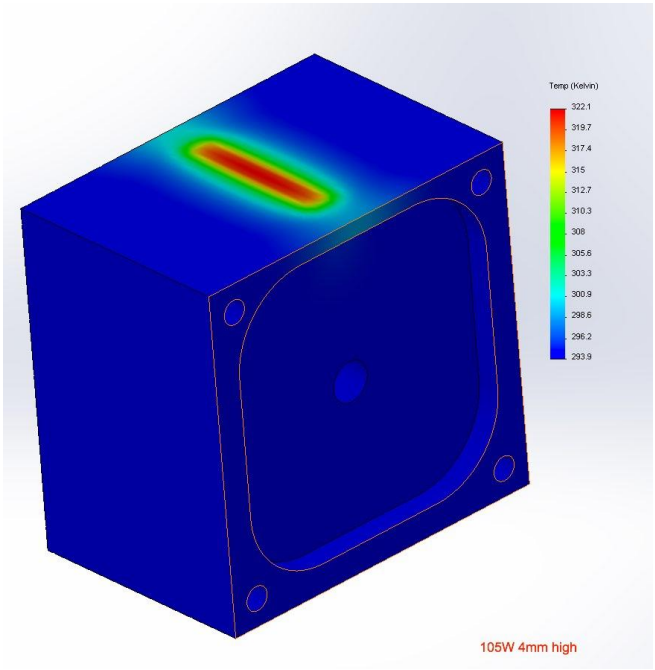

Figure 20: Monochromator crystal exposed to a beam 20 mm wide (0.64 mrad) by 4 mm high (0.13 mrad) using a uniform loading with a total exposure of 105 W. For a typical coolant flow of 4 litres/min. a 30 °C temperature raise is predicted by Finite Element analysis.

In summary, the use of water-cooling isn't suitable for all operational conditions particularly if full use is made of the available divergence. When the full vertical divergence is transmitted to the monochromator the thermal bump generated will result in slope errors that are large compared to the acceptance angle of the second monochromator crystal resulting in significant loss (25% or more) of monochromatic flux at the sample. For operation with a reduced fan of radiation (similar to the current situation at BM26A) the current cooling scheme would suffice. Please note that even under the most unfavourable conditions no damage will occur to the monochromator when using the existing water-cooling scheme.

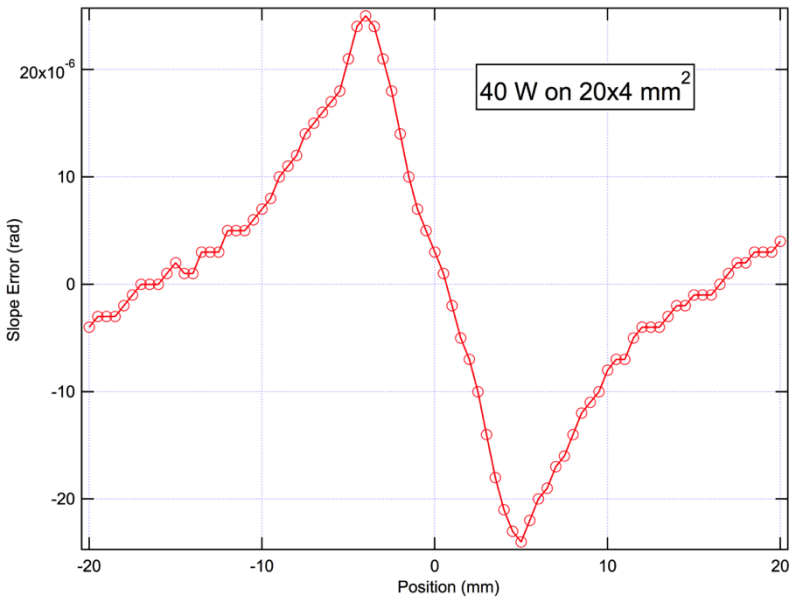

Figure 21: Slope error corresponding to heat loading as per figure 19 but with 40 W. Slope errors were calculated by inputting the temperature profile predicted by FE calculations in a static displacement calculation. A maximum slope error of 25 µrad is found which compares to 35 µrad at 105W.

ⓘ *Optimising the monochromator cooling scheme should be considered. In the literature two methods of improving the direct water-cooling scheme have been reported. These methods consist of micro-channel or pin-post structures buried just below the surface resulting a more efficient way to extract heat and these have been implemented at power densities of up to 5 W/mm^2 albeit with some residual strain (larger angular Darwin widths) in the crystal due to the way it is manufactured [6].*

Moving to liquid nitrogen cooling is often used at insertion device beamlines. Because the total power loading is relatively small an indirect cooling scheme that *removes issues with vacuum seals and vibrations due to the high pressure of the coolant is favoured*. Since the ESRF has a good knowledge of and infrastructure for liquid nitrogen cooling this change is straightforward without any technical risks.

6. Diagnostics

Beam diagnostics will be of great benefit to smooth beamline operation and quality of beam provision to the users. Energy scans require multiple motor scans to keep the beam at a fixed height. Large changes in energy will, in addition to the DCM adjustments, require tilt and mirror coating changes. Availability of diagnostics enables a high level of automation of beamline operations.

- The following parameters should be monitored:
- White beam position upstream of VCM
- Intensity downstream of DCM using diode
- Beam position/Intensity upstream of sample position
- Wavefront monitor
- Fluorescence screens/ slits with fluorescence strips
- High resolution beam imager
- Knife edge scanning stage with piezo for sample stage
- Set of vacuum compatible distance sensors with large bandwidth for monitoring DCM xtals

Measurement of the beam position at several points along the beamline facilitates automatic alignment of key optical components. An intensity monitor placed at the exit of the DCM is a very useful option and can provide a control input into an automatic monochromator stabilisation system. During experiments at the Ti-edge a novel stabilisation method was trialled successfully allowing both stabilisation of the monochromator and beam position at the sample [7]. A wide acceptance, achromatic intensity monitor was recently installed at BM26B which could provide the

A wavefront monitor consisting of a water-cooled micro pinhole array that can be inserted just upstream of the VCM is a very useful tool to diagnose whether the beam is properly collimated or whether any of the optical components suffer from misalignment. By recording the array of pencil-like beams at various points along the beamlne an accurate recording is made of the wavefront as it travels down the beamline. With a suitable arangement of the pinholes the system would also provide information regarding the coherent fraction of the beam.
Another solution to measure the wavefront of the beam is to use a grating interferometer that uses a 2D or chessboard pattern. This approach has been used to measure thermal bumps on optical components [8].

A portable knife-edge scanner using a piezo stage is particularly useful to measure micrometre -sized beams at the sample position. To monitor motions and vibrations in vacuum a set of three interferometers is needed to diagnose stability of the monochromator axes.

For accurate white beam power measurements it is helpful to have a calorimeter (copper block with thermocouple) that can be moved into the beam for a brief period.

☒ *Will there be access to white beam (x-ray) monitors at the front-end (inside the tunnel)?*

7. End station

Experiments at this beamline are relatively short (sometimes a day or less) which means that the experiments hutch should support quick changeover between experiments so that a minimum amount of time is lost getting the beamline ready for new users. With beamline alignment and beam energy changes quick and smooth, the hutch layout should allow co-existence of two or more measurement setups. For example, a suitably sized experiments hutch would have two or more setups in series or in parallel (optics dependent). This approach could be combined with one in which several setups are in parallel sitting on a common slide. Any switchover would therefore be quick by removing the need for lengthy re-alignment cycles. Particularly in the case for experiments that use complex post focusing and detector setups this approach using two large platforms will provide significant gains. Flexible sample positioning and how to allow for a variety of sample environments (cryostats, ovens, gas cells, etc.) has already been addressed in the existing setup. A standardised sample (chamber) kinematic mount is an obvious development that has been implemented.

Moving to a new bending magnet port will provide more space around the sample in which there will be access from three sides as opposed to two in the current situation at BM26A. A larger experiments hutch provides beamline scientists with more freedom to switch experimental setups or to have several setups in line so that a simple refocusing of the beam would remove the need for removing equipment from the hutch. Simultaneous XAFS and SAXS experiments will allow longer camera lengths increasing the accessible length scale.

The additional space also allows x-ray emission spectroscopy setups using wavelength dispersive setups either in von Hamos or in Rowland geometries to be placed on one side of the sample leaving the fluorescence detector stationary on the other. A dedicated polarisation analyser and a dedicated two-theta arm would further extend the range of measurement techniques.

Preliminary considerations for the requirements for the experiments hutch:

- Lifting table
- Optional X-ray optics (e.g. harmonics rejecting mirror system and/or KB)
- Set of Reference foils
- Three Ionisation chambers, gas lines, HV supplies and programmable low-noise amplifiers
- State of the art Fluorescence detectors and electronics
- Cryostat
- High precision sample stages
- Capillary holders
- Optical spectroscopy (Confocal Raman system, IR, visible)
- Crane (500 kg)
- ….

A further important point is that of hutch temperature control. Working with micrometre-sized beams requires stable sample mounts. Thermal differences less than a degree will already result in movements of the order of the beam size. The older type hutches restrict airflow resulting in local hot spots near heat generating equipment. In the newer hutches the airflow is improved using a diffusor. Efforts should be made to locate heat-generating equipment as much as possible outside the experiments hutch.

8. Detectors

The key detectors for the spectroscopy beamline are a multi-element fluorescence detector and a set of good ionisation chambers. The current 9-element Germanium fluorescence detector is rather old and no longer state of the art. To remain competitive a new multi element fluorescence detector from Canberra (HPGe) is required that provides a fourfold increase in solid angle captured by the detector - improving signal to noise significantly. This detector should be combined with the latest generation of read-out systems. Two different readout systems (Quantum Detectors and XIA) are available and a further study is required to decide which system is most suitable for DUBBLE. At DUBBLE tests are ongoing with the (mini)EXPRESS3 system from Quantum Detectors in combination with a VORTEX EM system for use with low energy x-ray detection. If satisfactory, a similar system could also be used for the large fluorescence system with multiple channels.

For x-ray fluorescence experiments a high-purity Germanium detector is required. There is no alternative to cover the required large range of energies. Canberra has changed fabrication techniques to overcome the poor peak shape and efficiency below 3 keV. This new technology from Canberra is now available, called Ultra-LEGe, and promises good energy resolution over a significantly wider energy range (300 eV – 300 keV). This would be an ideal fit with the new beamline capabilities. A further choice is to go for a discrete or monolithic device. In the former case the detector is made up from individual elements separated by small gaps. Monolithic devices are integrated onto a single wafer allowing for a seemless array with no blind spots. Discrete devices have a slightly better energy resolution compared to monolithic ones but these can only be created in an array size of 32 elements whereas monolithic detectors are available up to 100 elements. For the monolithic sensors the newer EXPRESS4 system is more suitable. One of the key choices of interest is that of solid angle covered, energy resolution and count rate. For example, a smaller number of elements that cover the same solid angle featuring high count rates at an excellent energy resolution compared to one with more elements but with a reduced count rate and resolution would clearly be of more interest and probably also less expensive certainly when one considers the reduced cabling and electronics. For this perspective a detector that has more than 40 elements would simply be of little interest unless it would cover a significantly larger area. The monolithic detector features either 5x5 or 8x8 mm^2 individual elements. The discrete elements are round and feature a 50 mm^2 area, thus a 64 element sensor with 5x5 mm^2 elements would be similar in area as a 32 discrete element one.

Recently Canberra (now: Mirion) has been testing an improved Ge detector system (LeGe) that combines electric cooling with uptp 17 discrete sensors that feature a much improved energy resolution at significant count rates for a range of energies starting at 3 keV. To operate without LN_2 cooling brings benefit in terms of maintenance and infrastructure and frees up space near the detector. This development albeit with a lower number of sensors seems very interesting for the new beamline. They also offer an ultra-low energy (UleG) version that would work for photon energies starting at 300 eV. These options require further investigation in order to select a detector most suitable for the envisaged beamline.

For micro focus experiments where there is little space close to the sample, a Vortex detector should be used. This sensor is also preferred for experiments with low energy x-rays for which the Vortex outperforms the regular high purity Germanium-based Canberra system. Such a system is already available and has recently been upgraded with state of the art electronics.

For complementary techniques we would also require a detector to record small angle and/or diffraction patterns. Large angle scattering would be captured with a linear detector such as a Dectris Mythen detector. For the small angle measurements either a Pilatus3 or Eiger Dectris detector would be ideal. Currently BM26A does not have a dedicated 2D detector to record small angle scattering patterns and a Frelon system is used belonging to the ESRF detector pool. Since availability is not garanteed it is necessary to invest in a Dectris detector. With the extended energy range available a detector with a high-energy photon imaging capability such as the Dectris Pilatus3 R CdTe is advisable particularly if pair distribution (PDF) measurements and imaging of bulk samples are required. The

Quantum Efficiency for the CdTe version of the Pilatus3 is high for photon energies of upto 60 keV. Almost four times higher in energy than the standard Silicon version.

For imaging with chemical contrast several approaches can be followed. For example, a high-resolution indirect imaging camera in absorption geometry would map chemical elements in either a 2D manner by recording a series of images as a function of x-ray energy. Such a scheme could be extended to 3D using tomographic methods. Also, a colour x-ray imaging technology could be used in a fluorescence setup similarly either in 2D or 3D (SLCAM or Medipix3RX). Such technology is rather new and there are currently a couple of systems available that could be considered for use with the new beamline depending on user demand.

9. Beamline Control Software

DUBBLE has invested a significant amount of effort in adopting the GDA software to control the energy scans and detector readout. As such GDA is able to operate in the SPEC software environment that performs lower level functionality. It should be relatively straightforward to integrate new detectors and electronics for which others have developed suitable drivers/servers. Most modern control system software make use of dedicated server code for devices such as motor control, detector control/readout, *etc*. These codes should be placed on a dedicated server system which has the ability to manage several network ports including some high-speed (10Gb/s) ones needed for some detector readout systems.

The transition to GDA has not been straightforward and lengthy but paid off such that the EXAFS station is now fully running a GDA based software for data collection. The main reason is that at the lower level the beamline still runs SPEC and GDA had to be adapted to make the change from EPICS to SPEC. Once SPEC becomes obsolete it will be necessary to adapt the existing GDA implementation but this task is already underway. The main application in terms of user operation is a GUI for doing typical spectroscopy data collection in which the x-ray energy is varied whilst collecting data from a range of sensors and beam intensity readings.

It would make sense to stay close to the ESRF in terms of software especially at the low level (drivers, etc.) such that it will be easy to make use of local efforts (e.g. BLISS framework, Tango). One such capability would be to perform continuous scans of the energy during data collection and thus avoiding the current start-stop approach. An effort to clean up the internal structure of GDA is anticipated, integrating new devices such as detectors, introduction of advanced triggering schemes is overly complex and time consuming. It is proposed to adapt the BLISS framework to create a more graphical way of controlling objects such as motors whilst at the same time keeping scripting capability and GUI-based applications for ease of use.

What is currently lacking is a comprehensive beamline control and recording of all parameters. A simple beamline synoptic display should be created which includes slits, mono, mirrors, diagnostics and vacuum. This could be extended by detectors and other key beamline equipment. With this in place it should then be relatively straightforward to collect regular and comprehensive recordings to file. A further important change is to create an environment that allows easy extension and timing of experiments. All too often beamline software is not or poorly integrated with sample environment and detector setups making it hard or simply impossible to perform so of the more challenging experiments that rely on timing and multiple detector data recording.

Any beamline at the forefront of research will require dedicated staff to support software development. The use of an existing framework provides a good environment in which DUBBLE can benefit from software developed elsewhere and at the same time contribute to new developments in an efficient way. With the move to a new port this software implementation can take shape.

Software will play a key role in keeping the beamline productive and to introduce and integrating new techniques and sufficient staff time needs to be allocated to support this activity. More use must be made of so-called pseudo motors so that users are relieved from performing manual adjustments to related axes.

Entangled with the software effort are the systems that it runs on and the systems that are controlled by it. A *decentralised* approach is called for. For stepper motor control the ICEPAP system is well suited allowing a large variety of stepper motors to be controlled over the network so that controllers can be based at various locations. DC motor control will need to be covered by other electronics. DUBBLE has already invested into McLennan controllers but these will not be suitable for direct driven axis or for advanced continuous scanning applications.

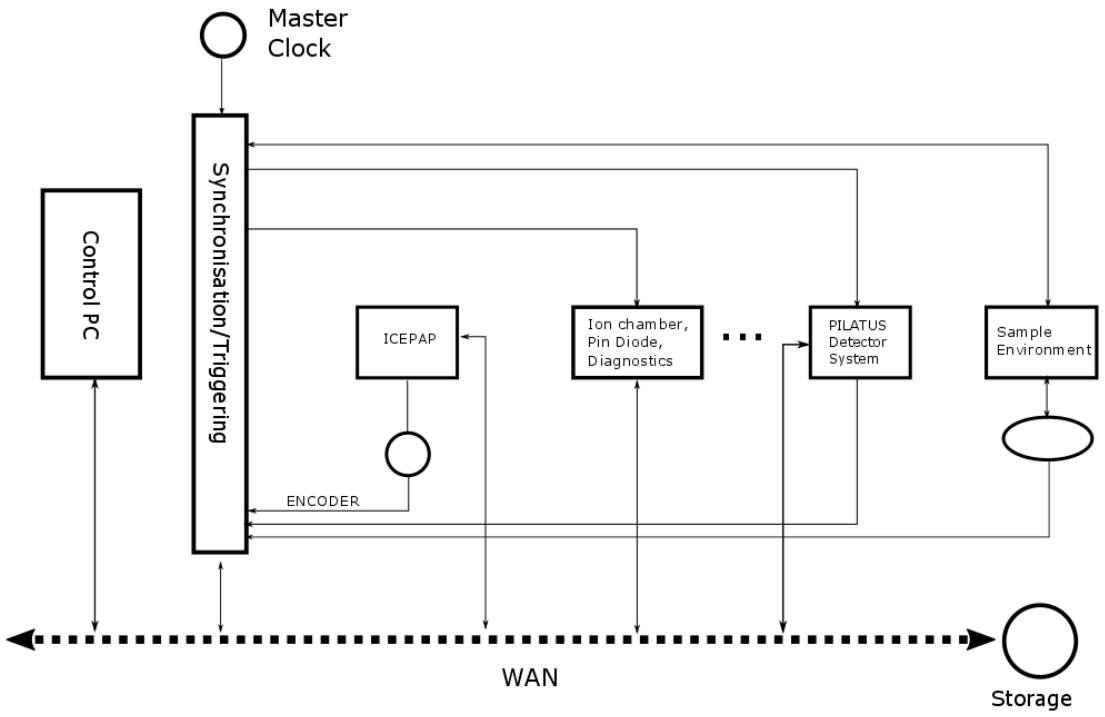

Figure 22: Overview of beamline control system. A decentralised approach in which a beamline control computer communicates with a range of systems responsible for motor control, data acquisition, detectors, etc. 2D detectors that generate large quantities of data store these directly to dedicated storage using high bandwidth paths not indicated in this diagram. From this diagram it is clear that the triggering and synchronisation unit should be able to generate precise timing to the various devices but also be able to read various timing signals from motors, detectors and sample environment controllers. The master clock could be a free running oscillator or a clock that is synchronised with the synchrotron RF system.

Overall this strategy increases flexibility and reduces overall wiring considerably. Recording of Voltages, Currents, Temperatures etc. can be done through network-based instrumentation. Although there already is a significant amount of VME based electronics available they are rather large and their availability after 2020 is uncertain. For certain data acquisition applications, however, their use might be the best best option for the short term and as such they could be made to comply with the decentralised approach provided suitable software is available.

Secondary bus systems or low-speed serial connections (GPIB, RS232, RS485) should be avoided. If needed these interfaces should be converted using suitable network adaptors.

10. Conclusions

The presented beamline layout consists of a well-proven concept in which focusing elements are separated from elements that select photon energy. Through the use of collimating mirror and selected filter materials of the full source spectrum can be restricted such that the monochromator heat load is minimised. The proposed design is makes the best use of the energy range and expected photon flux and is tailored for giving users a significantly wider range of photon energies at higher photon fluxes with a flexible approach to focusing such that it is easy to go from large to microfocused beam size. Energy scans will be faster using detectors that offer a significantly higher sensitivity particularly for fluorescence detection. Full use will be made of the microfocusing option by creating a flexible sample stage for 3D mapping of the chemical composition of samples using a confocal and tomographic facility.

Ray trace studies have highlighted the requirement for sub-microradian slope errors for collimating and focusing mirrors if source limited focal spot sizes are to be obtained. Also mirror bending mechanisms and gravity compensating mirror mounts are important for maintaining source brilliance. The existing mirrors feature rather large slope errors and would therefore result in larger focal spots as shown in this document. If preservation of the source brilliance is important either new mirrors should be used or the old ones should be re-polished/recoated to provide sub-microradian slope errors of 0.6 µrad or better.

Another area for attention concerns the most appropriate monochromator cooling system. The current direct water-cooled crystal will result in loss of monochromatic beam flux due to thermal deformations when exposed by a beam size that can be focused by the focusing mirror. With the use of filters the heat load can be reduced to acceptable levels whilst using direct water-cooling but for access to the highest possible photon flux a liquid nitrogen cooling is required.

From the ray tracing calculations it is clear that alignment of the beamline components to the central axis of the fan of radiation as produced by the 2PW insertion device is rather important because of the nature of the 2PW in which there are two source points thatare spatially separated. An effort should be made to create reference points to allow accurate beamline component placement.

The significant increase in available flux density at the sample will benefit experiments in spatial and temporal resolution in particular. Performing energy scans faster by two or three orders of magnitude will allow a big improvement of following the time evolution of chemical reactions or phase transitions.

Similarity of the proposed beamline concept with the existing BM26A beamline will enable reuse of many components such as slits, vacuum vessels, support structures and vacuum pumps. Beamline electronics such as motor drives have had the benefit of recent upgrades and can be used as is.

The current 9-element HpGe fluorescence detector is beyond its serviceable life with two of the 9 elements failing and must be replaced in order to remain competitive. DUBBLE currently has no backup solution. Modern systems collect larger solid angles at higher energy resolution even at high count rates and allow therefore more sensitive and faster measurements.

11. References

[1] K. Klementiev and R. Chernikov, (2014) Proc. of SPIE Vol. 9209 92090A-1 (doi: 10.1117/12.2061400).

[2] J. Chavanne, ESRF document 01-15/IDM/ version 0, unpublished (2015).

[3] I.K. Robinson, Z. Kristallogr. Suppl. (2008) **27**, 27-35 (doi:10.1524/zksu.2009.0005).

[4] A.J. Dent et al., Journal of Physics: Conference Series **430** (2013) 012023 (doi:10.1088/1742-6596/430/1/012023).

[5] A. MacDowell *et al.*, J. Synchrotron Rad. (2004) **11**, 447–455 (doi: 10.1107/S0909049504024835).

[6] S. van Dijken and R. van Silfhout, AIP Conf. Proc. (2000) **521**, 304-307 (doi:10.1063/1.1291805).

[7] R. van Silfhout *et al.*, J. Synchrotron Rad. (2014) **21**, 401–408 (doi:10.1107/S1600577513034747).

[8] S. Rutishauser *et al.,* J. Synchrotron Rad. (2013) **20**, 300-305 (doi:10.1107/S0909049513001817).

[i] Slope errors down to 0.25 urad are offered although no costing estimates are currently available.